Detection and Quantification of Drusen in Retinal Fundus Images

A Dissertation submitted in fulfillment of the requirements for the Degree of

MASTER OF ENGINEERING

in

Electronic Instrumentation & Control Engineering

Submitted by

Kajal Kumari
Regd. No.: 801351007

Under the Guidance of

Dr. DEEPTI MITTAL
Assistant Professor, EIED

2015

Electrical and Instrumentation Engineering Department
Thapar University, Patiala
(Declared as Deemed-to-be-University u/s 3 of the UGC Act., 1956)
Post Bag No. 32, Patiala – 147004
Punjab (India)

DECLARATION

I hereby certify that the work which is presented in dissertation entitled, **"DETECTION AND QUANTIFICATION OF DRUSEN IN RETINAL FUNDUS IMAGES"**, in partial fulfillment of the requirements for the award of the degree of Master of Engineering in Electronic Instrumentation and Control, submitted to Electrical & Instrumentation Engineering Department of Thapar University, Patiala is as authentic record of my own work carried under the supervision of Dr.Deepti Mittal. It refers others researcher's work which are duly listed in the reference section. The matter contained in this dissertation has not been submitted, neither in part nor in full to any other degree to any other university or institute except as reported in text and references.

Place: Patiala

Date: 13/07/15

(KAJAL KUMARI)

This is to certify that the above statement made by the candidate is correct and true to the best of my knowledge and belief.

(Dr. DEEPTI MITTAL)
Assistant Professor
Electrical & Instrumentation Engineering Department
Thapar University, Patiala

Countersigned By:

(Dr. RAVINDER AGGARWAL)
Professor & Head
Electrical & Instrumentation Engineering Department
Thapar University, Patiala

(Dr. S.S. BHATIA)
Sr. Professor & Dean
Academic Affairs
Thapar University, Patiala

ACKNOWLEDGEMENT

In pursuit of this academic endeavour, I feel that I have been singularly fortunate because inspiration, guidance, direction, cooperation, love and care - all came in my way in abundance and it seems almost an impossible task for me to acknowledge the same in adequate term.

I am very thankful to the Director of Thapar University, **Dr. Prakash Gopalan,** and our Head of the Department, **Dr. Ravinder Agarwal**, Department of Electrical and Instrumentation Engineering for their support during the research work.

Also, I shall be failing in my duty if I do not record my profound sense of indebtedness and heartfelt gratitude to my supervisor, **Dr. Deepti Mittal**, Assistant Professor, Department of Electrical and Instrumentation Engineering, Thapar University, Patiala, who guided and inspired me in pursuance of this work. It was her able supervision, advice, and guidance from the very early stage of this research as well as giving me extraordinary experiences throughout the work which has resulted in fruitful outcome. I feel bereft of words to acknowledge her contribution to shape my academic perceptivity.

I feel thankful to the entire faculty and staff of the Department of Electrical and Instrumentation Engineering. I would also like to thank my friends who devoted their valuable time and helped me in all possible ways towards successful completion of this work. I thank all those who have contributed directly or indirectly to this work.
Lastly, I would like to thank my parents for their unconditional support and encouragement.

Kajal Kumari

801351007

TABLE OF CONTENTS

LIST OF TABLES

LIST OF FIGURES

NOMENCLATURE

UN – United Nation

WHO – World Health Organization

AMD – Age Related Macular Degeneration

OCT – Optical Coherence Tomography

ICG – Indocyanine Green

FAF – Fundus Autofluorescence

CARMS – Clinical Age-related Maculopathy Grading System

AREDS – Age-related Eye Disease Study

RPE – Retinal Pigment Epithelium

CNV – Choroidal Neovascularization

GLCM – Grey Level Co-occurrence Matrix

FFNN – Feed Forward Neural Network

AM-FM – Amplitude Modulation-Frequency Modulation

RGB – Red, Green, Blue

HSV – Hue, Saturation, Value

OHTA - Office of Health Technology Assessment

SVDD – Support Vector Data Descriptor

DWT- Discrete Wavelet Transform

PNN- Probabilistic Neural Network

HOS- Higher Order Spectra

FD- Fractal Dimension

ROC- Receiver Operating Curve

AHE- Adaptive Histogram Equalization

ABSTRACT

Drusen are common features of the aging macula, caused by accumulation of extra cellular materials and fatty deposits beneath the retinal surface, visible in retinal fundus images as yellow-white spots. In the ophthalmologists' opinion, the evaluation of total number and area of drusen in a sequence of images taken during a treatment will help to understand the disease progression and the extent of its effect on the eye. However, this evaluation is fastidious, tiresome and difficult to reproduce when performed manually.

A literature review on automated drusen detection showed that the works already published were limited to drusen segmentation and quantification using limited information and also few of them provided grading of Age-related macular degeneration (AMD). The purpose of this work is to propose two automated method to quantify and grade the severity of AMD using advanced digital image processing techniques.

Method 1 presents an automated technique for segmentation and quantitative analysis of drusen based on: First, region-based statistical analysis which corrects the non-uniform illumination of background, enhances local intensity, minimizes image noise, segments image through Otsu's threshold in addition to morphological operation and hence computes area and edge of the detected drusen. Second, pixel-wise feature are examined that helps to extract the features of overlapped components through weighted centroid and standard deviation. It makes counting of number of drusen easy. Method 2 presents an automated method to detect and segment drusen in retinal fundus images using (i) gradient based segmentation to find true edges of drusen, (ii) connected component labeling to remove suspicious pixels from drusen region and (iii) edge linking to connect all labeled pixels into a meaningful boundary. Both methodologies have been applied and tested on two publicly available retinal image datasets i.e. Structured Analysis of retina (STARE) and Automated Retinal Image Analysis (ARIA), acquired with the aid of a digital fundus camera.

These methodologies are evaluated to improve the pixel-to-pixel analysis by comparing the segmented results with ground truth and validated by using different statistical analysis.

From the results of these studies it can be concluded that the methodologies proposed are capable to automatically measure drusen area, size and number in an accurate and reproducible process. Also, the thesis proposes grading of AMD to evaluate the stages of macular degeneration so that it can be treated at time to stop the progression of AMD.

Chapter 1

INTRODUCTION

1.1 Overview

The retinal Fundus photograph is widely used in the screening, diagnosis and treatment of various eye disease like Age-related macular degeneration, diabetic retinopathy etc. Age-related macular degeneration (AMD) has been reported as the main cause of vision loss in the developing countries by World Health Organization [1]. It is the most common cause of visual impairment in older adults of age 50 and above [2]. Currently the UN estimates the number of people with AMD are about 20-25 million worldwide. WHO estimated it as 8 million people with severe visual impairment i.e. AMD was found to be second leading cause of severe vision loss after cataract. Prevalence of AMD in people of age 75 year and more varies from 1.2% to 29.3% in different population [3]. Three population based studies; the Beaver Dam eye study, Blue Mountain eye study and the Rotterdam study report the overall prevalence rates to be 1.7% in US, 1.4% in Australia and 1.2% in Netherlands respectively [5]. About 20-55% of Asian patients are affected with exudative AMD. In south India, the prevalence is 1.1% whereas, in north India the prevalence rate is 4.7% [6]. The number of people with this condition is expected to increase approximately 2.5 fold in those aged 60 years over the next fifteen years [6-7]. It is mainly caused by life-style changes and its symptoms should be visible in a retinal examination. Medical image analysis and processing has great significance in the field of medicine, especially in non-invasive treatment and clinical study. Normally fundus images are manually graded by trained clinicians is a time-consuming, tiresome and resource-intensive process. A computer-aided fundus image analysis could provide an immediate detection and characterization of retinal features prior to specialist inspection. With the increasing size and number of medical images of eye, the use of computers in facilitating their processing and analysis has become necessary. In particular, computer algorithms for the delineation of anatomical structures problems and other regions of interests are a key component in assisting and automatic specific radiological tasks. Hence the use of image processing techniques for automating the analysis of these images will certainly increase the process reproducibility

and provide quantitative data to the ophthalmologist, enabling him to focus his attention on the diagnosis.

The aim of this thesis is to harness and expand the capabilities of digital fundus cameras in order to create an inexpensive and high-throughput automated system to screen and diagnose age related retinal disease (e.g. Age-related macular degeneration) to assess the drusen affected area from fundus images. A system able to correctly referring patients to an expert if a retina condition is detected would be of great help for older people with AMD of age 50 or above, who can be screened remotely and inexpensively and ophthalmologists that would not otherwise be able to meet the health demands of an increasing AMD population. The state of the art image processing techniques, semi-automated and automated algorithms have been researched and an automated technique have been developed and tested to reach this goal.

1.2 Aims and objectives

The aim of this work is to develop a set of tools for the retina screening of diabetic patients uniquely with colour fundus images. Main objectives of this thesis are mentioned below:

- **Objective 1**: Develop an automated algorithm to assess the quality of fundus images.
- **Objective 2**: Develop an automated algorithm to segment drusen and detect boundary of drusen in the colored fundus images.
- **Objective 3**: Develop an algorithm to quantify drusen in the context of other state of the art techniques.
- **Objective 3**: Develop an algorithm to grade the severity of AMD in the context of other state of the art techniques.
- **Objective 4**: Develop an algorithm to classify drusen into its subtypes.
- **Objective 5**: Evaluate the algorithms in the context of drusen screening.

In addition to the previous objectives, the research of other techniques in the context of macular degeneration screening was encouraged. Therefore, after meeting the initial objectives automated methods are developed to detect boundary of drusen. A complete algorithm to detect drusen and grade the severity of AMD from the fundus images was

developed. Techniques to extend the functionality of standard fundus cameras with multiple images were investigated and two different methods were developed: one to detect the defected part of macula i.e. drusen and one to diagnose the severity level of AMD.

1.3 Thesis Overview

This thesis is divided into six chapters. An outline of each one follows:

- **Chapter 2** introduces the basic biological information required to fully comprehend the medical terms and techniques used throughout the thesis; it introduces the existing systems used to capture the image of the retina and different image modalities.

- **Chapter 3** it presents the common image analysis techniques employed for the analysis of the eye fundus and the existing automated and semi-automated approaches for drusen detection to diagnose the AMD.

- **Chapter 4** describes two different methods to segment drusen using two publicly available datasets which is able to automatically process retinal images, quantify the area affected by drusen and grade the severity of disease, using digital image processing techniques. The complexity of these images along with the low contrast and non-uniform illumination make the development of these techniques a difficult task. The work is contribution of medicine and engineering fields, in the sense the tools developed will certainly improve the clinicians work by freeing them from the manual markings and the engineering field which will benefit from the developments of new image processing algorithms, as well as case study for other biomedical applications of image processing.

- **Chapter 5** presents an algorithm to automatically evaluate the performance of drusen detection method. The algorithm is tested on two publicly available datasets which allows the comparison with other existing drusen segmentation techniques developed by other researchers.

- **Chapter 6** deals with the results and discussion.

- **Chapter 7** deals with conclusion and future scope.

This work has dedicated especial focus on AMD and in particular drusen which are one of its early signs. These are yellow spots which appear in the retina surface and can vary in size depending on their type and disease evolution. For the ophthalmologists the quantitative evaluation of the total area affected by drusen in a sequence of images taken during a long term treatment will positively help in assessing its effectiveness. Currently, to quantify these areas manual marking of drusen is done which requires attention, precision and time from the ophthalmologists, which is incompatible with their daily interventions. The subjectivity of the criterion to detect drusen also affects the reproducibility of the technique and increases the variability among ophthalmologists analysis. Hence in this work two different automated techniques are proposed to detect and diagnose the AMD.

Chapter – 2

BACKGROUND AND SIGNIFICANCE

This chapter introduces the medical aspects required to fully comprehend the significance of fundus image analysis in AMD patients. First, a general overview of the eye and the retina is given. Second, different retina abnormalities are described. Then, different imaging modalities are discussed. Particular attention is given to the lesions directly related to retinal diseases typical of patients with AMD of age 50 and above. Finally, two aspects of retina screening in AMD patients are described: the various manual protocols available and current completely automated techniques for retina screening.

1 The Eye and Retina

1.1 Eye's Anatomy

Out of five senses, Vision i.e. eye is arguably the most important sense organ in the human body. We rely on our eyes to provide most of the information due to quality and precision of the signals it captures and by reduction of quality of life within its absence. In the optical science, the human eye is often compared to a camera because of the way it processes light into information understandable by the brain [9]. Its functioning is similar to conventional image capture systems due to its lenses that refract and focus the incoming light in the sensorial region. A camera uses the film to create a picture, whereas the eye uses a specialized layer of cells, called the retina, to produce an image. The eye has ability to focus on a wide range of objects having different sizes, luminosity and contrast at a high speed, composed of different structures among these components most important are discussed below [10-11]. Figure 2.1 shows a schematic view of the anatomy of eye.

Aqueous Humour: The aqueous humour is a jelly-like substance located in the anterior chamber of the eye that keeps the front of eye firm and slightly curved. The interior surface of the eye, opposite the lens, is called the fundus [12].

Choroid: The choroid layer is located behind the retina and absorbs unused radiation.

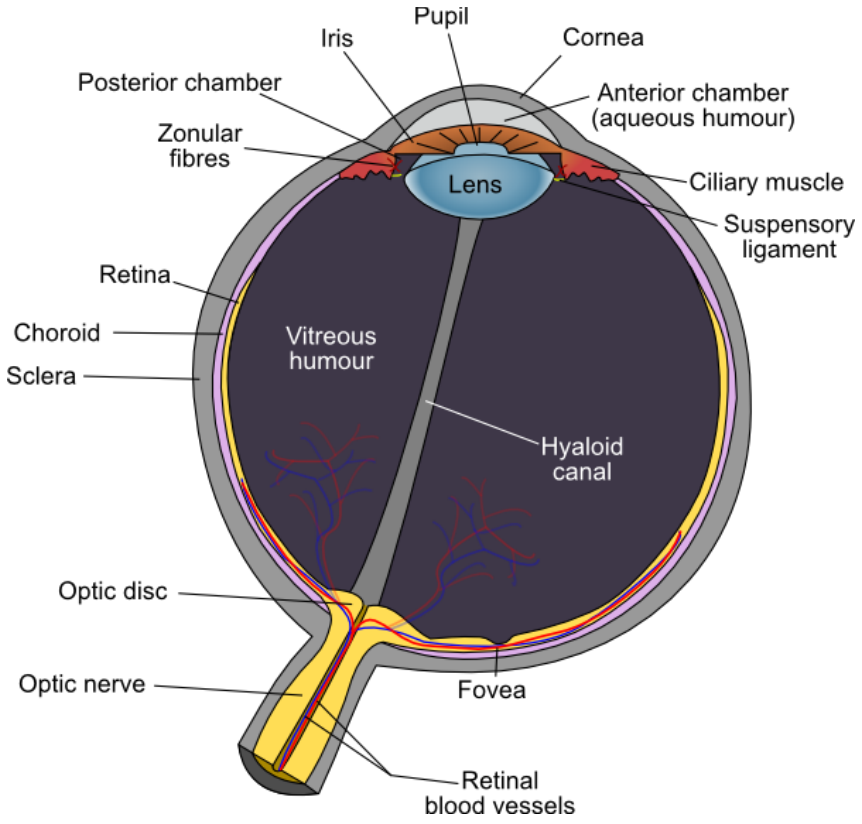

Figure 2.1 Global eye's anatomy

Ciliary Muscle: The ciliary muscle is a ring-shaped muscle attached to the iris. It is important because contraction and relaxation of the ciliary muscle controls the shape of the lens.

Cornea: The cornea is a strong clear bulge located at the front of the eye (where it replaces the sclera - that forms the outside surface of the rest of the eye). The front surface of the adult cornea has a radius of approximately 8mm. The cornea contributes to the image-forming process by refracting light entering the eye.

Fovea: The fovea is a small depression (approx. 1.5 mm in diameter) in the retina. This is the part of the retina in which high-resolution vision of fine detail is possible.

Hyaloid: The hyaloid diaphragm divides the aqueous humour from the vitreous humour.

Iris: The iris is a diaphragm of variable size whose function is to adjust the size of the pupil to regulate the amount of light admitted into the eye. The iris is the colored part of the eye.

Lens: The lens of the eye is a flexible unit that consists of layers of tissue enclosed in a tough capsule. It is suspended from the ciliary muscles by the zonule fibers.

Optic Nerve: The optic nerve is the second cranial nerve and is responsible for vision. Each nerve contains approx. one million fibers transmitting information from the rod and cone cells of the retina.

Papilla: The papilla is also known as the "blind spot" and is located at the position from which the optic nerve leaves the retina.

Pupil: The pupil is the aperture through which light - and hence the images we "see" and "perceive" enters the eye. This is formed by the iris. As the size of the iris increases (or decreases) the size of the pupil decreases (or increases) correspondingly.

Retina: The retina may be described as the "screen" on which an image is formed by light that has passed into the eye via the cornea, aqueous humour, pupil, lens, then the hyaloid and finally the vitreous humour before reaching the retina. The retina contains photosensitive elements (called rods and cones) that convert the light they detect into nerve impulses that are then sent onto the brain along the optic nerve. It is divided into following layers as shown in in Fig. 2.2, discussed below [10].

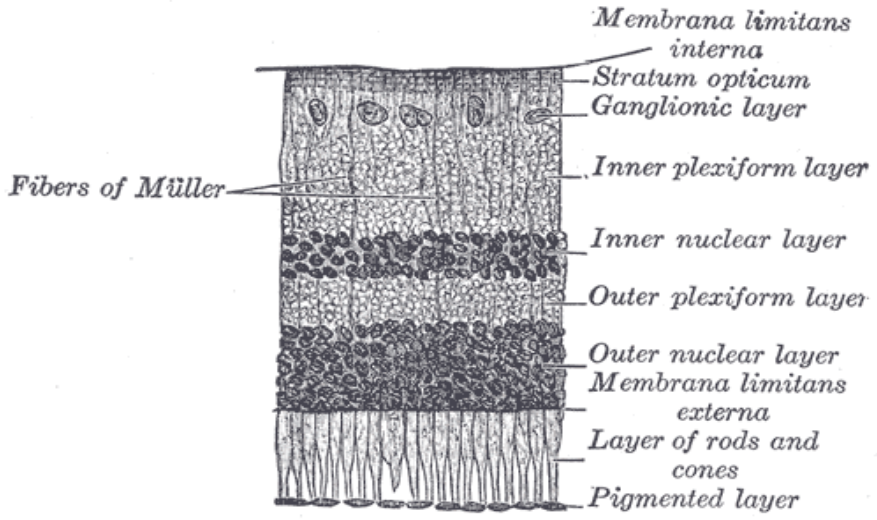

Figure 2.2: Retinal Layers distribution

1. **Internal limiting membrane** or membrane, limitans or internal.
2. **Nerve fibre layer** contains the axons of the ganglion cells, which transmit the signals to the visual cortex of the brain. This layer is much thicker in younger retinas and it slowly thins the more it ages. As the blood vessels in the inner layer, this fibre is not present over the fovea in order to permit all the photons to reach the rods without obstacles.
3. **Ganglion cell layer** contains the body of the ganglion cells.
4. **Inner plexiform layer** contains the axons of the bipolar cells and the amacrine cells.
5. **Inner nuclear layer** contains the cell bodies of the bipolar and horizontal cells.
6. **Outer plexiform layer** contains the inner segments of the photoreceptor cells and the dendrites of the horizontal cells.
7. **Outer nuclear layer** contains the body of photoreceptor cells.
8. **External limiting membrane** or membrane, limitans or external.
9. **Pigment epithelium**. It is the last layer of the retina. It is the one that give different colour (pigment) to each human retina.
10. **Bruch's membrane**. First layer of the choroid.
11. **Capillary choroid** contains all the blood vessels that provide the primary source of retina nutrients.

12. Choroid plexus. Last layer of the choroid.

Sclera: The sclera is a tough white sheath around the outside of the eye-ball. This is the part of the eye that is referred to by the colloquial terms "white of the eye".

Visual Axis: A simple definition of the visual axis is a straight line that passes through both the centre of the pupil and the centre of the fovea. However, there is also a stricter definition (in terms of nodal points) which is important for specialists in optics and related subjects.

Vitreous Humour: The vitreous humour (also known as the "vitreous body") is a jelly-like substance.

Zonules: The zonules (or "zonule fibers") attach the lens to the ciliary muscles.

1.2 Retinal Imaging Modalities

Many of the pathologies that affect the retina can be visible in retina surface, hidden in a deeper layer require different diagnostic exams to correlate information between them and produce a reliable and well supported diagnosis. Ophthalmologists use ophthalmic (or eye) photography to visualize changes in retinal layer helps in recording the ocular condition over time, provide diagnostic information and also used extensively in basic scientific research and clinical trials that investigate new treatments for debilitating eye diseases. Ophthalmologists conventionally imaged the eye using two types of ophthalmoscopes: direct and indirect which allowed for the determination of the health of the retina and vitreous humour.

1.2.1 Direct Ophthalmoscope: -

It is the first instrument used for retinal examination, about the size of a small flashlight with several lenses that can magnify up to about 15 times. This instrument is used for routine examinations, because it is practical and portable, used for early detection of retinal abnormalities [13].

1.2.2 Indirect Ophthalmoscope: -

It is also known as fundus camera, where the fundus is the interior surface of the eye. A fundus camera provides an upright, magnified view of the fundus of the interior surface of the eye: the retina, optic disc, macula, and posterior pole (i.e. the fundus). A typical camera views 30 to 50 degrees of retinal area, with a magnification of 2.5x, and allows some modification of this relationship through zoom or auxiliary lenses from 15 degrees which provides 5x magnification to 140 degrees with a wide angle lens which minimizes the image by half [14].

1.2.3 Optical Coherence Tomography (OCT): -

Optical coherence tomography (OCT) is a non-destructive imaging technique that uses interferometry techniques to measure the time of flight of the light backscattering through the retina, typically employing near-infrared light. It captures micrometer-resolution, three-dimensional images from within optical scattering media (e.g., biological tissue). The use of relatively long wavelength light allows it to penetrate into the scattering medium. Optical coherence tomography (OCT) systems are employed in diverse applications, notably in ophthalmology where it can be used to obtain detailed images from within the retina [15], as shown in Fig. 2.3.

1.2.4 Fluorescein Green Angiography: -

Angiography is a diagnostic test used by ophthalmologists to take images of the eye's back portion and is especially useful in finding damage to the blood vessels, which nourishes the retina.

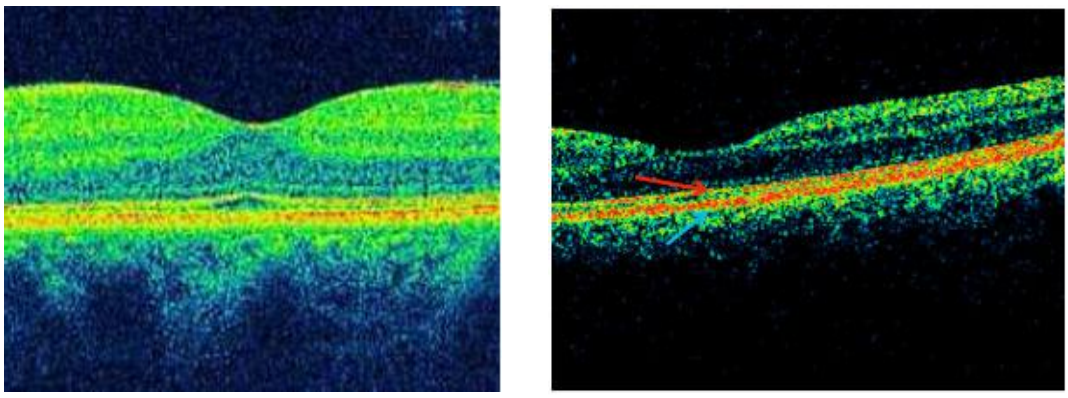

Figure 2.3: (a) Normal OCT scan showing human retina in cross-section (b) OCT scan showing macular degeneration

There are two types of angiography: fluorescein and indocyanine green (ICG). Fluorescein angiography is used primarily to study blood circulation in and just beneath the surface of the retina. The purpose of either type of angiography is to determine whether there are irregularities in the circulatory system of the retina. Several serious eye disorders, such as diabetic retinopathy, affect retinal circulation and are usually studied with the fluorescein procedure.

1.2.5 Indocyanine Green (ICG) Angiography: -

ICG angiography is a method which captures an image of the deeper choroidal vessels. The problems, such as age-related macular degeneration, are caused by leakage from the deeper choroidal blood vessels can be assessed by using physical properties of ICG [mora]. In these cases, the ICG procedure can provide additional information, which may not be available through a fluorescein angiography [16].

1.2.6 Fundus Auto Fluorescence (FAF): -

Fundus Auto fluorescence (FAF) represents an imaging modality capable of reflecting the morphological changes associated with the common downstream pathogenetic pathway. It allows for documenting the presence of fluorophores in the human eye in a non-time consuming and noninvasive way. Fluorophores are chemical structures that possess fluorescent properties when exposed to light of an appropriate wavelength. Fluorescence occurs when these molecules absorb electromagnetic energy, which excites them to a higher energy state and triggers the emission of light at wavelengths longer than the excitation source. FAF is used to record fluorescence that may occur naturally in the eye or accumulate as a byproduct of a disease process. It is suitable to detect optic nerve drusen, astrocytic hamartomas, lipofuscin pigments in the retina, and the aging crystalline lens because it is believed that all exhibit natural fluorescence [17].

1.2.7 Slit-Lamp Photography: -

Slit-lamp photography is the photography of the structures of the eye with a specially designed horizontally mounted microscope. The primary illumination for the

microscope is produced by a light which can be adjusted from a very broad pattern to a very narrow slit of light, derives its name. The slit can be used to isolate structures in the eye. The photograph above illustrates the use of a narrow slit of light to identify the surfaces of the cornea and lens of the eye.

1.2.8 Thermal/Infrared (IR) Imaging Modality: -

It provides a non-invasive, in vivo method to diagnose early changes in RPE/Bruch membrane. It minimizes the light scattering through cloudy media. It enhances the quality of an image and provides additional information regarding CNV and the character of drusen and sub-retinal deposits [56]. IR imaging detects pathology despite the presence of hemorrhage or cataracts that may be undetected in others. Digital fundus camera cannot provide useful IR images due to its limitation i.e. unable to separate reflected and scattered light due to its scattering property which makes it noisy, consisting low detail definition [18].

Table 2.1: Pros and cons of imaging modalities

IMAGING MODALITIES/ TECHNIQUES	**PROS**	**CONS**
FUNDUS IMAGING	• Provides better information for smaller drusen • Useful for screening and early detection of AMD	• Cannot visualize metabolic changes at the level of photoreceptors/RPE
FUNDUS AUTOFLUORESCENCE	• Able to visualize metabolic changes at the level of photoreceptors/RPE • Can measure size and shape of GA areas	• Takes more time in area calculation of RPE lost cell at the GA margin
INFRARED	• Detect RPE alteration • Detect area of RPE lost cell earlier than FAF • Less harmful for eyes	• Not applicable for CNV detection
SD-OCT	• Better than other imaging modalities at capturing information non-invasively • Can provide quantitative and	• Shows better performance for larger drusen only i.e. advanced AMD • Cannot identify the border of

	reproducible data to follow the progression of disease • Provide better identification of normal and pathological structure in patient with poor media clarity	drusen precisely
OCT	• Can visualize dry AMD	• Slower than SD-OCT in case of noise handling
FA	• Can detect CNV	• Poor transmission of fluorescence through ocular media opacification, fundus pigmentation and pathological manifestation • Having limitation in imaging choroidal circulation
ICG ANGIOGRAPHY	• Useful for detecting CNV in neovascular AMD.	• Not suitable for smaller drusen

2 Retinal imaging for AMD grading

Retinal color fundus imaging has been widely used for AMD grading. A number of grading protocols has been established for grading drusen and identify the stage of AMD using color fundus imaging. Among them Wisconsin Age-related Maculopathy Grading System, the International Classification and Grading system for Age-related maculopathy and Age-related Macular Degeneration and its modified version as well as Age-related macular disease study classification system and Clinical Age-related Maculopathy grading system (CARMS) are widely used.

2.1 The Wisconsin Age-related Maculopathy Grading System

It is a grid of three circles and four radial lines, concentric with the centre of the macula, is placed over fundus photographs which are mounted on clear plastic sheets and placed on a fluorescent viewing box and retro-illuminated using light with a Kelvin rating of approximately 6200^{o}. The circles have radii corresponding to 500, 1500 and 3000 μm on the fundus. The grid defines nine subsections of fundus; three sets of open circles printed on clear plastic are used to estimate the size of drusen, area covered by drusen, and areas of pigmentation [19].

2.2 The International Classification and grading system for Age-related Maculopathy and Age-related Macular Degeneration

In this system three circles are centred on the foveola, of diameters corresponding to 1000 μm, 3000 μm and 6000 μm on the retina. Lesions are graded within each of the central, inner, or outer circles. In this system five open circles printed on clear plastic can be used to estimate the size of drusen, area affected by drusen, and the area with decreased or increased pigmentation. Drusen present within the outer circle are classed as most common type. Large drusen (> 63 μm) are counted separately but small drusen are not. In this system it is difficult to detect choroidal vessels and determine the edges of GA in smaller areas [20].

2.3 Modified version of the International Classification and Grading system for Age-related Maculopathy and Age-related Macular Degeneration

In this subfields are defined creating a circle with a radius corresponding to 3000 μm on the foveola and bisecting it into semicircles nasal or temporal to the foveola. A circle with radius corresponding to 1500 μm centred on the foveola was superimposed. Thus inner nasal, inner temporal, outer nasal and outer temporal were created. Number of drusen greater than 63μm, size of the largest drusen, predominated drusen type, area covered by drusen, confluence of drusen, focal hyperpigmentation, presence of geography atrophy and presence of other atrophy are determined for each of these four subfields [21].

2.4 Age-related Macular Disease Study Classification system

The Age-related eye disease study (AREDS) was a randomized controlled trial (RCT) designed to evaluate the effect of a high-dose vitamin C, E, beta-carotene and zinc supplement on the progression of AMD progression and visual acuity [22]. It classified AMD into different classes according to size of drusen.

2.5 Clinical age-related maculopathy grading system (CARMS)

CARMS is a modification of the AREDS grading system [23-24]. Within this system, macular characterized are graded within a 3000 μm radius centred on the foveal

centre. Eyes with extremely small drusen ($\geq$ 15 small drusen; <63 μm), non-extensive intermediate drusen (< 20 drusen; $\geq$63 but <125 μm), or pigment abnormalities associated with AMD are assigned a grade of two. Eyes with extensive intermediate or large drusen ($\geq$125 μm) are assigned a grade of three. Eyes with GA receive a grade of four. If evidence of RPE detachment and/or choroidal nonvascular membrane was found, a grade of five is assigned. Advanced AMD is defined as grades of four and five.

The grading scales described above were designed for use with stereoscopic fundus photographs. The methods mainly used computer software tools that a grader uses to manually count the drusen through drawing different sizes of circles in the software interface. This is very time consuming, tedious and prone to human error. Digital retinal photography is increasingly used in clinical practice and research which promotes use of three grading scales with digital imaging.

3 Retinal Diseases Related with Age

Blindness is one of the most undesirable consequences of any eye disease. There are several types of retinal eye diseases like Diabetic Retionpathy, Cataract, Glucoma, Ocular Tumour and Age-Related Macular Degeneration. Out of all these diseases, Age-related Macular Degeneration is one of the most common causes for irreversible blindness in the developed countries.

4.1 Age-Related Macular Degeneration

Age-related macular degeneration is the leading cause of irreversible vision loss in people of age 50 years or older. According to World Health Organization (WHO) it is the third cause of irreversible blindness [1]. It is a disease that causes progressive damage to the macula, leading to distorted vision and ultimately to a complete loss of central vision. As the name itself suggests AMD is age related, common among people of age 50 and older [2]. In case of AMD, peripheral vision is usually retained and therefore total blindness does not typically occur. The profiles of patients that have higher probability of developing AMD are as follows:

- Age – signs of AMD present in people of aged between 55 and 64 is 14%, between 65 and 75 is 20% and people over 75 is 37% [25].

- Gender – more common with women than with men due to partial fact that women live longer than men [25].
- Race – more common in Caucasians than other races due to the pigment in eye colour, diets and sun exposure [26].
- Eye color – more common with people with blue eyes may be due to exposure to ultraviolet light [27].
- Genetics – AMD is associated with genetic factor. If someone in the family contracted AMD it is likely that some of their descendants may develop it also [27].

Apart from this, there are also some risk factors which can be genesis of AMD. These are explained below:

- AMD in one eye – If one of the eyes is affected with AMD the probability to develop in the other eye is higher [28].
- Cardiovascular problems – It was found a higher incidence of AMD on people having hypertension [29].
- Dietary habits – The dietary habits may also influence negatively or positively the risk of AMD. It was found that a fat dietary increases the risk, while a dietary based on fish reduces it [30].
- Exposure to Sunlight – The long exposure to sunlight, especially to ultraviolet without protective sunglasses can increase the risk of AMD [31].

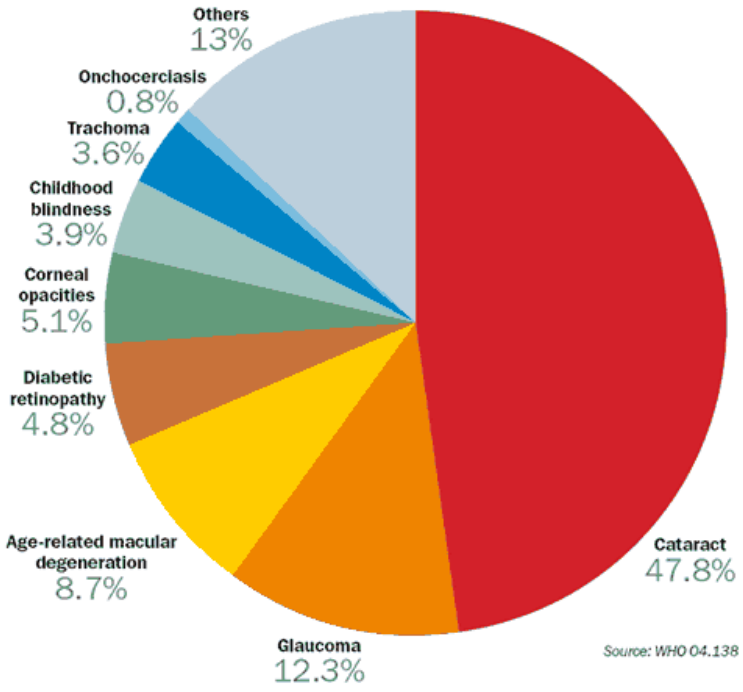

Figure 2.4: Global causes of blindness as a percentage of total blindness in 2002

- Smoking – Smoking is being highly correlated with the presence of AMD. The risk of AMD is two to three times higher in smokers than non-smokers [32].
- Drusen – These are small lipid deposits that appear in retina surface and can lead to AMD. It contributed to development of AMD [33].

Symptoms of AMD are like a distorted vision and/or occlusions in the formed image as exampled in Fig. 2.5. If it is not treated at time then these symptoms will increase progressively until a total occlusion. It is characterized by a detachment of the macula from choroid causes deficient of nutrition of the macular cells causing their death progressively.

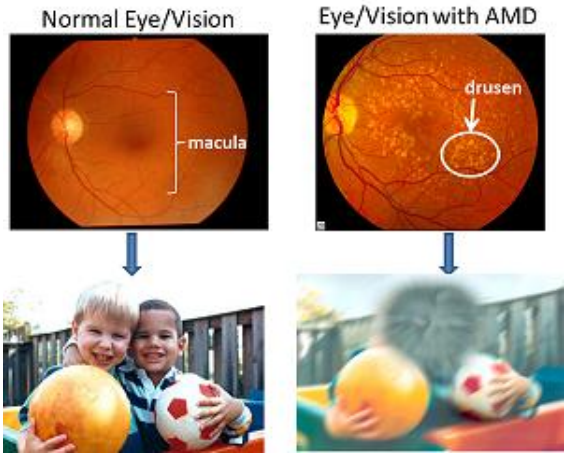

Figure 2.5: Visual perception of a patient with AMD or without AMD

4.1.1 Types of AMD

The stages of AMD can be defined on the basis of severity of AMD pathologies. It is basically of two types.

a) Dry AMD

Dry AMD having two stages: early and intermediate in which the light-sensitive cells in the macula become changed and gradually blurring central vision of the affected eye due to accumulation of waste material under the RPE forming yellowish deposits called drusen. These waste materials slow down the transport of nutrients and wastes by the RPE due to detachment of macula from choroid. As the retinal pigment epithelium (RPE) continues to slow down in its transport of nutrients and wastes, the overlying photoreceptors become damaged. In the intermediate stage, the size and number of drusen and geographic atrophies in the macula increases. In case of late dry AMD, gradual breakdown of the light-sensitive cells in the macula occur that convey visual information to the brain, and of the supporting tissue beneath the macula occurs with progressive atrophy of the RPE, choriocapillaris and photoreceptors. Around 80-90% of all diagnosed patients are affected by late dry AMD [2] as shown in Fig. 2.6 (c).

b) Wet AMD

It occurs when abnormal blood vessels behind the retina start to grow under the macula. The proliferation of these new blood vessels is called choroidal neovascularization (CNV). These can provoke macular detachment and bleeding causes

loss of vision. It usually appears in fundus images as darker regions due to bleeding as shown in fig. These darker regions form blind spots due to CNV [2] as shown in Fig. 2.6 (b).

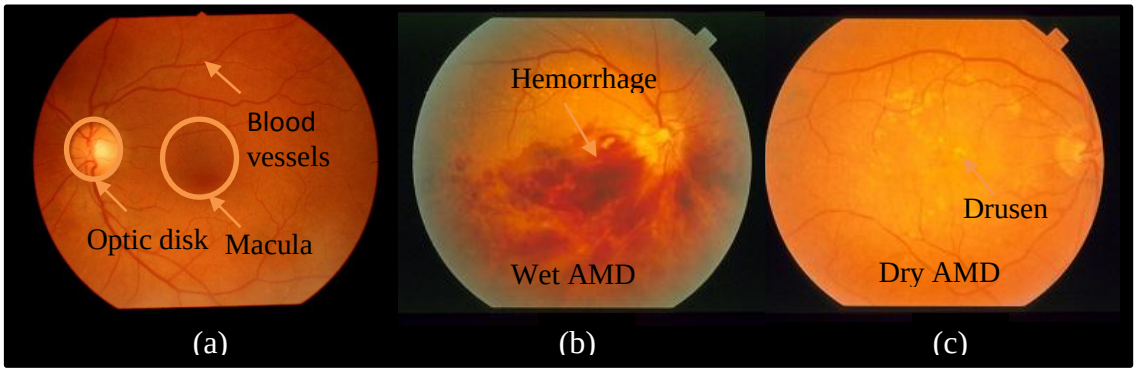

Figure 2.6: (a) normal eye (b) Wet AMD (c) Dry AMD

4.2 Drusen as a risk factor for AMD

The drusen are pale yellow deposits of cholesterol and other extracellular materials in retina between the RPE and the Bruch's membrane as shown in Fig 2.7. These are considered as a strong risk factor for AMD [33]. Drusen appears as yellowish, cloudy bright blobs in a retinal image, appear scattered or concentrated, depending on the stage of AMD. In the early stages the accumulation and size of drusen is usually small. There is little or no impact of it on vision because in these cases human brain compensates the small size abnormalities. In late stages, drusen deposits grow in accumulation and size causes blurred vision. The patients generally needs more light and will often indicate a loss of central vision in macular region.

Drusen are the earliest clinical sign of early dry AMD and are categorized on the basis of size and appearance. Clinically, they are divided into two types: hard and soft drusen [2, 34]. Hard drusen are mainly characterized by small sized spots with less than 63µm of diameter and sharp edges, whereas soft drusen are medium sized spots between 63µm and 250µm of diameter with smooth edges, which can be confluent with irregular shapes as shown in Fig. 2.7 (a) and (b).

The detection of drusen and control of its progression in early stages is important to reduce the risk of degeneration and consequently the development of AMD.

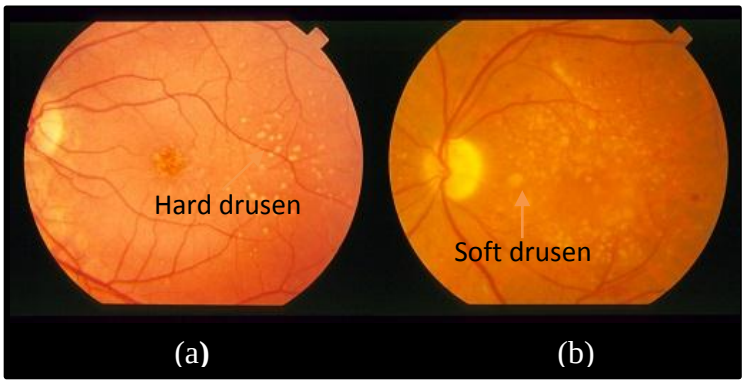

Figure 2.7: (a) hard drusen (b) soft drusen

Chapter – 3

LITERATURE REVIEW

The automatic detection of drusen has been object of research for almost three decades and the research paper dated since 1986 can be found. The challenge is to develop methods using digital image processing that can consistently detect drusen on retinal fundus images, having different contrast and non-uniform illumination on its surface. These methods are not only used to detect the presence or absence of drusen, but also to quantify it according to its size, number, area and type. The ability to study the progression of drusen on a series of images during a treatment without changing the detection criteria is very useful for the ophthalmology specialist, who can accurately detect if the disease is stable or progressive.

The main purpose of researches on drusen detection is to find the Standard technique which help in drusen quantification for finding the severity of AMD. However, the subjectivity of the analysis and the need of complementary exams to support the analysis are difficult to achieve consent among ophthalmologists to find the technique which is most reliable. Drusen detection and grading of AMD using conventional methods are time-consuming, tiresome and fastidious process. Hence, ophthalmologists are requiring user friendly, fast and accurate tools that can reproduce their analyses over their patient retinal images. Therefore, a number of semi-automated and automated techniques are developed for drusen detection. In this chapter a chronological overview of existing state of art algorithms using semi-automated and automated methods to detect drusen is discussed for the following aspects: texture, thresholding, clustering, edge based, quantification and quality assessment. Additionally, comparisons of existing drusen segmentation techniques with their pros and cons are presented. are presented on the following sections.

3.1 Drusen Detection

The drusen detection method aimed to quantify the presence of abnormalities like drusen and characterize them according to their shape and size. Detection of hard and soft drusen is difficult because of their differences, contour smoothness and shape which is

hard to be recognized by computer software hence it is distinguished manually, a tiresome or time taking procedure. In this chapter, some of the semi-automatic and automatic techniques or methods are discussed that were developed in past to detect and quantify the drusen.

3.1.1 Texture based drusen segmentation

Texture generally describes the property of surfaces and scenes, measured over image intensities. If the appropriate texture methods are applied on drusen, which is generally brighter in view shows different texture response than the background. Using this hypothesis, researchers have applied a number of methods based on Gabor filter, wavelet feature extraction, amplitude modulation – frequency modulation, GLCM based feature extraction, multi scale feature extraction and entropy based feature extraction as summarizes in Table 3.1.

Brandon and Hoover [35] developed a multi-level method with wavelet-based feature extraction for detection and classification of drusen. In this Mexican hat wavelet is applied to obtain four one dimensional (1D) responses and pixel's "wavelet signature", is computed from the product of four 1D responses. Pixels are classified by using Feed Forward Neural Network (FFNN). From the pixel-level segmented image, region-level classification is achieved which further help in area classification and image level classification to obtain an overall size and area of drusen.

Parvathi and Devi [36] developed a method for drusen detection, based on a bank of Log-Gabor filters and topographic models. Edge of the drusen is detected by applying a bank of Gabor filters with different scale and orientations on retinal green channel image to capture the high frequency components i.e. edge of drusen.

Lee et al. [37] proposed a method for disease and non-disease retina which is based on texture information and clustering to select drusen and non drusen images. A feature space is constructed to cluster the texture based on similarity by using Multiscale top-hat filter along with other non-homogenous texture descriptor such as multi-channel wavelet. The clustering starts with a low frequency texture subspace to assign similarity assignments then membership assignments are refined by incorporating higher frequency subspaces during clustering. An unsupervised learning method is applied to separate the feature space into non overlapping clusters to learn a partition function which is further

used to assign the cluster membership for a new test sample based on closest similarity match with highest probability.

Barriga et al. [38] proposed a method for lesion phenotyping on AMD to develop an automated AMD grading system. Amplitude modulation – frequency modulation (AM-FM) is used to generate multi-scale features for classifying pathological structures such as vessels, retinal background, hard and soft drusen. AM-FM methods are applied on at different scales for representing an image input image as a sum of AM-FM components. Eleven different combinations of scales are used for extracting the dominant AM-FM. This method is applied on three color spaces: RGB, HSV and the OHTA. Partial least square is used to classify the features.

Freund et al. [39] proposed a method for AMD and non-AMD image classification based on Multiscale analysis and Support Vector Data Description (SVDD). It comprises intensity based equalization algorithm, Mexican hat wavelet to derive a set of feature values for each pixels in the image and SVDD algorithm along with Gaussian radial basis function to classify the pixels into a binary image. Blood vessels are removed by morphological erosion and dilation.

Kose et al. [40] proposed a method for AMD detection based on identification of healthy and degenerative regions in the retina. Statistical properties of healthy textures are used and thresholding is done to segment the region. Inverse segmentation is implemented to obtain the area of degeneration.

Agurto et al. [41] evaluated the performance of AM-FM algorithm on retinal photographs. This method is same as Barriga et al. [82] method but the difference is that Agurto evaluate the performance of AM-FM algorithm by providing ground truth for the presence of pathological conditions, including drusen, micro aneurysms, hemorrhages, exudates and others.

Priya and Aruna [42] proposed a method for dry and wet AMD detection using Discrete Wavelet Transform (DWT) and Probabilistic Neural Network (PNN). DWT is used to obtain the coefficients in horizontal, vertical and diagonal directions. Kirsch template is used to obtain the edge information including direction and PNN is used classify the dry and wet AMD.

Prasath and Ramaya [43] proposed a method comprises novel medical decision support system for automatic detection of drusen from retinal images. It involves preprocessing for non-uniform correction and contrast enhancement. Morphological top-hat transform is used to detect the blood vessels and selected features are properly labelled to segment the macula region. This study presents a new method to quantitatively measure drusen texture features based on Gray-level Co-occurrence Matrix (GLCM).

Mookiah et al. [44] proposed an automated dry AMD screening method using fundus images. It uses various entropies, higher order spectra (HOS) bispectra features, Fractional dimension (FD) and Gabor Wavelet features extracted from greyscale fundus images. The features are ranked using t-test, ROC curve based, Wisconsin ranking methods and other. The non-linear features extracted using HOS and Gabor Wavelet is able to identify the abrupt changes in the normal and dry AMD images.

Table 3.1: Summary of Texture based drusen detection methods applied on retinal fundus images

NAME OF THE AUTHOR	YEAR	TECHNIQUE USED	PROS	CONS
Brandon and Hoover	2003	• Mexican hat wavelet • Feed Forward Neural Network	• Segment drusen or non-drusen images • Categorized segmented region as normal, large few drusen, large many drusen, fine few drusen, fine many drusen and abnormal drusen	• Achieved only 87% accuracy for classifying drusen and non-drusen • 71% accuracy for small or large drusen classification • Unable to classify hard and soft drusen
Parvathi and Devi	2007	• Log-Gabor filter • Thresholding • Model based drusen detection	• No pre-processing was required • Classified drusen or non-drusen images	• Performance was not evaluated
Lee et. al	2008	• Multiscale Top-hat filter • Structural similarity clustering	• Presented a learning approach for non-homogenous texture discrimination • Classified drusen and non-drusen	• Accuracy varied from 71.7% to 92.2%. • Tested with small sample size • No grading was done

Barriga et. al	2009	• Multiscale feature selection through Amplitude Modulation-Frequency Modulation • ROI selection by partial least square • PLS clustering	• Achieved 100% accuracy in Classifying pathological structures such as vessels, retinal background, hard and soft drusen • Achieved 96% accuracy in classifying hard and soft drusen	• Classification of distinct and indistinct drusen was not carried out • Grading was not performed
Freund et. al	2009	• Multi scale analysis • Support vector machine	• Free from fundus variation	• One normal and six AMD fundus images were used for testing • No grading was performed
Kose et. al	2010	• Statistical texture properties • Thresholding • Edge based vessel detection	• Inverse segmentation was implemented to obtain small, medium and large area degeneration • Achieved 84.06-92.6 % accuracy for small area degeneration, 89.89-96.06% for medium area degeneration and 90.67-95.16% for large area degeneration	• Unable to report anything about distinct and indistinct drusen
Agurto et. al	2011	• Multiscale feature selection through Amplitude Modulation-Frequency Modulation • ROI selection • K-means clustering • 2-step PLS classifier	• Classified image as normal and abnormal • Evaluated drusen area • Evaluated performance of AM-FM algorithm	• Achieved an average accuracy of 73% • Grading was nor performed
Priya and Aruna	2011	• Discrete wavelet transform • Probabilistic neural network	• Classified dry and wet AMD • Tested on 100 images	• Achieved accuracy of performance evaluation parameters i.e. sensitivity,

				specificity and accuracy less than 96% • Drusen was not classified
Prasath and Ramaya	2015	• GLCM based texture feature extraction • Morphological top-hat transform	• Classified small, medium and large drusen • Achieved 98.05% accuracy	• Validated with 40 images • Severity of AMD was not analyzed
Mookiah et. al	2014	• Entropies • Higher order spectra (HOS) bispectra features • Fractional dimension • Gabor wavelet feature extraction • classification	• Achieved average classification accuracies of 90.19%, 95.07% and 95% using SVM classifier.	• Extracts only features of grey scale images • Grading was not performed

3.1.2 Thresholding-based drusen segmentation: -

Thresholding is a technique which converts an image into a binary image based on intensity or frequency to obtain the region of interest. There are number of techniques have been implemented for drusen segmentation based on thresholding as summarizes in Table 3.2.

Morgan et al. [45] proposed a method for extraction and quantification of macular drusen using retinal fundus images. Firstly, it applies median filter to reduce the impulse noise then it subdivides the image into several small regions and computed the mean pixel intensity value. To obtain the brighter pixel location a threshold value is computed from the adjacent region and pixel location. Macular region is selected manually from the digital image and the Polaroid prints to quantify the drusen areas.

Rapantzikos and Zervakis [46] proposed a method for drusen segmentation by using histogram-based adaptive local thresholding method which applies on enhanced

retinal images with uniform illumination. Homomorphic filtering is used for non-uniform illumination correction and a multilevel variant of histogram equalization is developed for contrast enhancement. Global thresholding is applied for testing symmetry or asymmetry and histogram adaptive thresholding is applied on local regions depending upon shape properties i.e. skewness and kurtosis etc.

Soliz et al. [47] developed a quantitative assessment method for maculopathy using color retinal images. Gaussian smoothing and probability based thresholding method is used to quantify drusen and assess longitudinal changes in retinal images presenting with maculopathy. It follows Wisconsin Age-Related Maculopathy Degeneration Grading Scheme.

Smith et al. [48] proposed a method for morphological analysis of drusen based on macular background reflectance thresholding. Initially non-uniform illumination due to retinal reflectance is corrected by a common shading correction method on each channel of RGB. The background pattern in the green channel is leveled by an algorithm based on the elliptically concentric geometry of the reflectance in the normal macula. The segmentation of drusen and area measurements in the central and middle subfields is performed by uniform thresholds.

Barakat and Madjarov [49] investigated a semiautomatic method on drusen quantification for clinical trials. A region of interest is defined by an operator using a user interface to allow the system to select the drusen region robustly. Variation of the brightness level is adjusted for increasing the efficiency of drusen detection. Then an intensity index is defined based on several cycles of drusen detection to optimize the algorithm's performance.

Smith et al. [50] developed an automated method to segment the drusen area. In this method the background is selected by Otsu method which is applied by dividing the image into two zones: central and middle zone. The sequential automated background leveling and histogram-based thresholding are applied to segment the drusen areas.

Liang et al. [51] developed a method for drusen detection which is based on macular region mapping, vessel removal and intensity thresholding. Edge detection algorithm is applied on red and green color channel which is further added to produce the

binary edges based on thresholding. Morphological dilation is applied to smooth the boundaries of the detected regions and produce the mask to remove the vessel region.

Sheeba and Vinayan [52] proposed a novel method for automatic detection of drusen exudate using retinal images. To segment the drusen from the retinal images enhancement and morphological operation is performed. The software Vision Assistant of Lab VIEW is used for the automatic detection and mapping of drusen deposits in the retinal images.

Prasath and Ramaya [53] developed an automated method for finding the position of optic disk and eliminating it, improve the drusen detection accuracy. The method starts with a color channel selection that provides a better contrast and reduces computational complexity. The contrast and illumination of the image is normalized by using adaptive histogram equalization (AHE) and homomorphic filtering respectively. The optic disk localization is achieved by active contour segmentation using morphological operator.

Kumari and Mittal [54] proposed an automated method for quantification of drusen. In this Otsu thresholding is used for segmentation of drusen. Non-uniform illumination is corrected by subtracting the background from original image. Pixel-wise feature is extracted for decomposing the overlapped drusen.

Table 3.2: Summary of thresholding based drusen segmentation

NAME OF THE AUTHOR	YEAR	TECHNIQUE USED	PROS	CONS
Morgan et. Al	1994	• Median filtering • Region subdivision • Intensity thresholding	• Provide extraction and quantification of macular drusen • Drusen area were detected	• A significant number of drusen area was miss calculated with up to 100% difference between manual and automated method
Rapantzikos and Zervakis	2001	• Homomorphic filtering • Histogram based adaptive local thresholding	• Achieved 100% accuracy in drusen pixel detection	• Unable to grade the AMD

Soliz et. al	2002	• Median filtering • Gaussian smoothing • probability based thresholding	• Developed a quantitative assessment method for detecting the drusen and its size	• Achieved 71% accuracy to quantify drusen and 67% accuracy in agreement between the graders on different drusen size • Severity of AMD was not evaluated
Smith et. al	2003	• Background levelling • Uniform thresholding	• Classified small, Intermediate and large drusen respectively	• Achieved Cohen's kappa statistics value of 0.61, 0.62 and 0.76 only for small, intermediate and large drusen respectively • Grading was not performed
Barakat and Madjarov	2004	• Region of interest selection • Intensity thresholding	• Sensitivity of 86% and specificity of 93% was measured on the basis of drusen area	• No grading was done to evaluate the severity of AMD
Smith et. al	2005	• Otsu's method for background selection • Intensity thresholding	• Drusen area was calculated • Sensitivity varied from 0.42 to 0.86 and specificity from 0.53 to 0.98	• No grading was done • Unable to identify types of drusen
Liang et. al	2010	• Edge based thresholding • Morphological dilation	• Edge of drusen was detected	• Achieved 75% sensitivity and specificity respectively • No quantification was performed
Sheeba andVinayan	2013	• LabVIEW • Gamma correction • Histogram based thresholding • Morphological operation	• Analyzed the extent and progress of AMD through LabVIEW • Detect border and area of drusen	• Database was not mentioned • Types of drusen was also not mentioned and classified

Prasath and Ramaya	2014	• Homomorphic filtering • Otsu's thresholding • Morphological operation.	Achieved an average accuracy of 4.9% and 93%. Drusen detection is improved by removing the optic disk.	Achieved an average FRR of 3.3% only. No grading is performed.
Kumari and Mittal	2015	• Otsu's thresholding • Morphological operation • Area based analysis • Region based properties • pixel-wise feature extraction	• Detect exact boundary of drusen	• Small drusen was missed out • No grading was performed

3.1.3 Clustering based drusen segmentation: -

Clustering is the task of assigning a set of objects into groups with similar nature than the other groups summarized in Table 3.3.

Hanafi et al. [55] developed an automated method for AMD and non-AMD image classification. It focused on feature vector generation from intensity distributions and spatial histograms.

Quellec et al. [56] proposed a method for the detection of drusen and other lesions based on a feature space which is automatically derived from a set of reference image samples. Factor analysis is used to derive the filters generating this feature space from reference samples. Then the image is classified using this feature space.

Raza et al. [57] proposed a method for drusen detection from the fundus images by using Gabor kernel based filter bank and eliminating spurious regions which may be confused with drusen. This method represents each region with a number of features and then applies hybrid classifier as an ensemble of Naïve Bayes and Support Vector Machine to classify these regions as drusen and non-drusen.

Zheng et al. [58] developed an automated method for drusen detection from color fundus photographs to automatically assess the risk for the development of AMD. This method incorporates learning based drusen detection and includes fundus image analysis

techniques for image denoising, illumination correction and color transfer. It incorporates both optimal color descriptors and robust Multiscale local image descriptors for drusen detection.

Hijazi et al. [59] developed a method which is based on spatial histogram and Case Base Reasoning approach for classifying image into AMD and non-AMD. Image is portioned into a number of regions after preprocessing and each region is represented in a spatial histogram. A class separability measure is applied for selecting the most appropriate spatial-histograms, each representing one image and stored in the form of time series curve as Case Base. Then the Case is classified by finding the most similar case in the Case Base.

Mookiah et al. [60] developed a method for automatic drusen detection using discrete wavelet based feature extraction. Features are then classified through supervised classification. The method was evaluated using 10-fold cross validation. Five supervised classifiers were used to compare the discrimination ability of the extracted features.

Table 3.3: Summary of clustering based drusen detection methods

NAME OF THE AUTHOR	YEAR	TECHNIQUE USED	PROS	CONS
Hanafi et. al	2010	• Spatial histogram • Similarity based classification	• Classified images into AMD and non- AMD	• Achieved 77% accuracy in classification
Quellec et. al	2011	• Factor analysis • Distance based clustering	• Achieved an accuracy of 0.85 in ROC curve making	• No grading was performed • Types of drusen was not identified
Raza et. al	2013	• Gabor kernel filter bank • Hybrid classifier	• Classified drusen and non-drusen images • Achieved an accuracy of 98%, sensitivity of 97% and specificity of 99% respectively	• Only STARE database was used • No grading was performed

Zheng et. Al	2013	• Pixel-wise feature extraction • Region based classification	• Classified AMD from color fundus photographs (CFPs) • Sensitivity varied from 0.82 to 0.85 • Accuracy varied from 0.80 to 0.86	• Specificity varied from 0.71 to 0.78 • Drusen was not classified and unable to identify the severity of AMD
Hijazi et. al	2013	• Hierarchical image decomposition • Weighted graph mining • Image portioning • Classification • SVM based feature selection	• Achieved 100% accuracy using LibSVM classifier • Grade the severity of AMD	• Achieved only 89% of sensitivity • Drusen was not quantified
Kaookiah et. al	2014	• Discrete wavelet based feature extraction • Supervised classification	• 184 features were extracted • SVM based classification achieved 93.70% accuracy and 91.11% sensitivity • Mean difference of AMDRI is 6.539 ± 1.911 and 2.265 ± 0.162	• No grading was performed
Mookiah et al.	2014	• Discrete Wavelet Transform • SVM classifier	• Classified normal and dry AMD • The method was evaluated using 10-fold cross validation • Five supervised classifier were used to compare the discrimination ability of extracted features	• Severity level of AMD was not provided • Quantification of drusen was not performed

3.1.4 Edge and template matching

Edge detection defines the set of pixels that form the border of a region that separates it from neighboring regions. This approach is used most frequently for segmenting images based on abrupt (local) changes in intensity summarized in Table 3.4.

Remeseiro et al. [61] developed a method for automatic drusen detection from digital images. The method applies template matching and threshold operation for drusen region selection. Two Gaussian templates are used to produce cross-correlation with the image region. A threshold is selected based on the empirical value and a seed point is selected to apply seeded region growing operation until no more pixels can be added to any existing region.

Mora et al. [62] proposed a method for automatic drusen detection and quantification using retinal images. An iterative cubic smoothing spline fitting method is applied for non-uniform illumination correction, a root mean square contrast calculation is applied for contrast normalization. Gradient based segmentation approach is used to isolate drusen.

Bhuiyan et al. [63] present a novel automated method for drusen detection and quantification which is used for initial screening of early stage of AMD or AMD progression. This method automatically determines the threshold intensity value by approximating the OD area information, blood vessel segmentation is based on texture property analysis in color retinal images. A Gaussian and LAB perpetually uniform color spaces with original RGB is used for texture feature extraction. A bank of Gabor energy filters are used to analyze the texture feature from which a feature vector is constructed for each pixel. The fuzzy C-Means clustering algorithm is used to classify the feature vectors into vessel or non-vessel based on texture properties. A morphological skeletonisation operation is applied on segmented image to extract vessel and Gaussian derivative is applied to produce the edge of the drusen.

Table 3.4: Summary of edge and template matching based drusen detection methods

NAME OF THE AUTHOR	YEAR	TECHNIQUE USED	PROS	CONS
Remeseiro et. al	2009	• Gaussian template matching • Thresholding	• Proposed a top-down strategy to detect drusen.	• Validated with four images. • Achieved only 83% sensitivity and 87% specificity

Mora et. al	2011	• Illumination correction • Normalization • Gaussian derivative	• Achieved specificity of 96% • Drusen area were detected	• Achieved sensitivity of 68% only • Only twenty-two retinal images were used for identification
Bhuiyan et. al	2013	• Gaussian derivative • Region growing	• Drusen detection and quantification was done • Achieved 100% accuracy	• Achieved sensitivity and specificity of 74.9% and 81.17% respectively • No grading was performed

Chapter – 4
METHODOLOGY

In this chapter two automated methods are employed for drusen detection, quantification and grading of AMD to further diagnose the disease, which is discussed below:

4.1 Method 1 [54]

The method is divided into four phases: Pre-processing, Drusen segmentation, Pixel wise feature extraction, and Quantification of drusen. As illustrated in Fig. 4.1, the integrated image analytics of applied system consists of several image processing procedures. These include retinal fundus image as an input. In order to detect drusen, green channel is selected because it having better contrast than other channels, correction of non-uniform illumination by creating an approximation of the background through morphological opening and then subtract this approximated image from original image, enhancement of image is done by automatic contrast enhancement, segmentation of image is done by Otsu's threshold, noise is removed by morphological operation. A label matrix is created after segmentation to visualize the drusen as a pseudo color indexed image. Decomposition of overlapped components in an image is obtained by calculating the object properties which are based on pixel-wise feature extraction through weighted centroid of mass. Weighted centroid is also used to locate the exact the position of spot that has been blurred over an image region by the image acquisition process. Edge of the drusen is detected by canny edge detector which classifies a pixel as an edge if the gradient magnitude of the pixel is larger than those of pixels at both its sides in the direction of maximum intensity change.

4.1.1 Selection

Green channel is selected from color retinal fundus images because it gives better contrast which helps in extracting brightest region from the background.

4.1.2 Non-uniform illumination correction

Retinal images having non-uniform illumination because these are acquired with digital fundus camera, which captures the illumination reflected from the retinal surface. There are also several other factors like curved surface of retina, pupil dilation, cataract & unexpected movement causes severe distortions in the resulting image. Background of an image having non-uniform illumination, hence to make background illumination more uniform, create an approximation of the background as a separate image by removing all the foreground using morphological opening. When this approximated image view as a surface it shows the variation of illumination. Now subtract this approximated image from the original image which will give a uniform image.

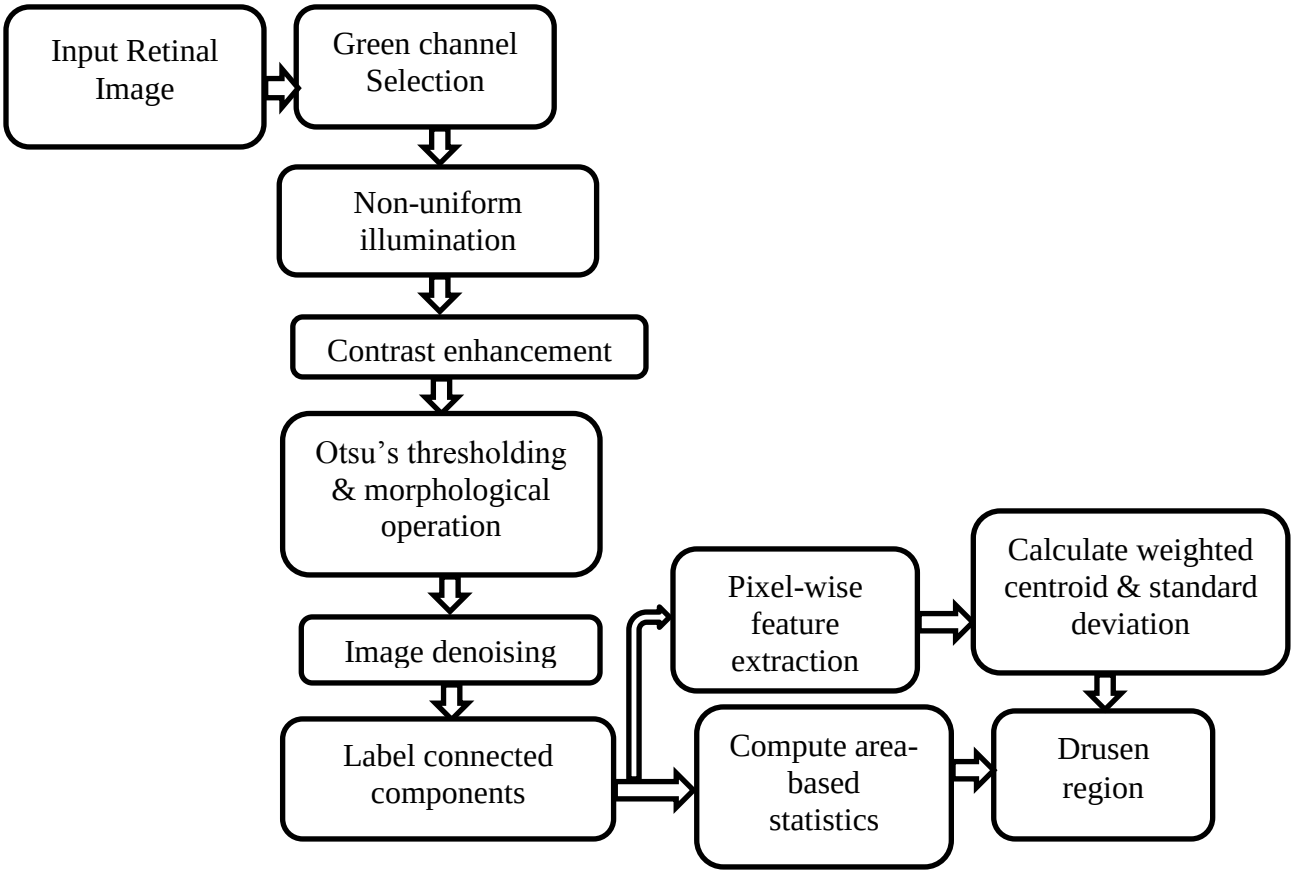

Figure 4.1: Flowchart of Method 1 for automated drusen detection

Morphology is a tool for extracting image components that are useful in representation and description of region shape. The opening operation has the effect of

removing objects that cannot completely contain the structuring element, in this erosion is followed by dilation as shown below.

$$Dilation, (I_m \oplus S_t)(x,y) = \max_{i,j}[I_m(x-i, y-j) + S_t(i,j)] \quad (4.1)$$

$$\text{Erosion}, (I_m \ominus S_t)(x,y) = \min_{i,j}[I_m(x+i, y+j) - S_t(i,j)] \quad (4.2)$$

$$Opening, \quad I_i \circ S_t = (I_m \ominus S_t) \oplus S_t \quad (4.3)$$

Where I_m is image on which we have to do the operation & S_t is the structuring element. I_i is the resultant image after opening operation. (x, y) is the co-ordinate of an image and (i, j) is the coordinate of structuring element.

4.1.3 Contrast Enhancement

Necessity of contrast enhancement arises due to non-ideal acquisition during imaging hence Automatic contrast enhancement is used. It is a technique for mapping an image's intensity value to a new range. In this technique the values in the intensity image $g(x, y)$ is transforms to values in $f(x, y)$ by mapping values between low and high to the values between bottom and top. The values below low and above high are clipped i.e. values below low map to bottom and those above high map to top.

4.1.4 Drusen detection

To efficiently detect drusen, a combination of mathematical morphology and Otsu's algorithm is used. Binarization of the retinal image is done by using Otsu's algorithm, to separate complex regions from the smooth ones. This technique partition the image into two classes $w_0 = \{0,1,2, \dots t\}$ and $w_i = \{t+1, t+2, \dots L-1\}$ at a gray level t, where L represents the total no. of gray levels of the image. Let n_i be the number of pixels at ith gray level, and the total no. of pixels in a given image be n. the probability of occurrence of gray level i is defined as $P_i = n_i/n$. The probabilities of the two classes w_0 and w_i are $q_1(t)$ and $q_2(t)$ are calculated, as shown in Eq. (4.4)

$$q_1(t) = \sum_{i=0}^{t} p_i \ , q_2(t) = \sum_{i=i+1}^{L-1} p_i \quad (4.4)$$

The mean of the classes are then computed as

$$\mu_j(t) = \sum_{i=0}^{t} iP_i/q_j(t) \tag{4.5}$$

Let σ_B^2 and σ_T^2be the between-class variance and total variance respectively. An optimal threshold t^* can be obtained by maximizing the between-class variance as given in Eq. (4.6).

$$t^* = Arg\left\{\max_{0 \le i \le L-1} (\sigma_B^2/\sigma_T^2)\right\} \tag{4.6}$$

After applying segmentation the largest connected region is marked as a candidate for drusen. The image obtained after segmentation having objects which can be referenced separately as shown in Eq. (4.7). Otsu's global thresholding technique has been used to make the proposed system robust and prevents the user intervention during the execution.

$$I_i(r,c) = \begin{cases} 1, & if\ I(r,c) \in object\ labeled\ 'i' \\ 0 & otherwise \end{cases} \tag{4.7}$$

$$where, r \in [0 \ldots Height - 1] and\ c \in [0 \ldots Width - 1]$$

Background noise will be removed through mathematical morphology as given in Eq. (4.1) and (4.2). Mathematical morphology also helps to remove the irrelevant vessels from the drusen region. A structuring element is used by selecting the size and shape of the neighborhood. In an image to add the pixels to the boundaries, dilation is used and to remove the pixels from the boundary erosion is used. The shape and size of the structuring element determines the number of pixels added or removed from the image. After detecting drusen a label matrix is created to display it as a pseudo colour indexed

image. Pseudo colour is used to compute total no. of drusen present in an image and then find area of each object through Eq. (4.8).

$$\text{Area, } A_i = \sum_{r=0}^{H-1} \sum_{c=0}^{W-1} I_i\,(r, c) \tag{4.8}$$

The area A_i is measured in pixels and it indicates the relative size of the object.

4.1.5 Pixel-wise feature extraction

In this step object properties is calculated by weighted centroid using pixel value of gray scale image. The (gray value weighted) center of mass is often useful to locate the exact position of a spot that has been 'blurred' over an image region by the image acquisition process. This will also help in decomposition of overlapped objects into individual particle. Hence exact number of drusen can be evaluated by an Eq. (4.9) and (4.10).

$$\bar{r_i} = \frac{1}{A_i} \sum_{r=0}^{H-1} \sum_{c=0}^{W-1} r I_i\,(r, c) \tag{4.9}$$

$$\bar{c_i} = \frac{1}{A_i} \sum_{r=0}^{H-1} \sum_{c=0}^{W-1} c I_i(r, c) \tag{4.10}$$

The Eq. (4.9) and (4.10) corresponds to the row and column where the centre of mass is located. This attribute will help to locate the objects in a bi-dimensional image.

$$f(x, y) = \sqrt{\frac{1}{mn-1} \sum_{(r,c)\in w} [g(r, c) - \frac{1}{mn-1} \sum_{(r,c)\in w} g(r, c)]^2} \tag{4.11}$$

Eq. (4.11) is used to calculate standard deviation. It is used for custom calculation based on pixel values of the original grey scale image. The 'pixel values' property returns a vector containing the grey scale values of pixels in a region. Where, $f(x, y)$ is the grey image on which standard deviation is represented. $g(r, c)$ is the binary image on which

standard deviation is calculated, *mn* represents the size of the image. Conventional edge detector is used to find the edge of the drusen which is basically canny edge detector.

4.2 Method 2

The proposed method to detect drusen and its boundaries consists of three phases named as (i) retinal image preprocessing, (ii) candidate drusen edge detection and (iii) boundary extraction of drusen. Fig. 3represents the summarized form of the proposed methodology in terms of complete flow diagram. Each step shown in the diagram are briefed further and presented below along with the performance evaluation parameters to evaluate the proposed method.

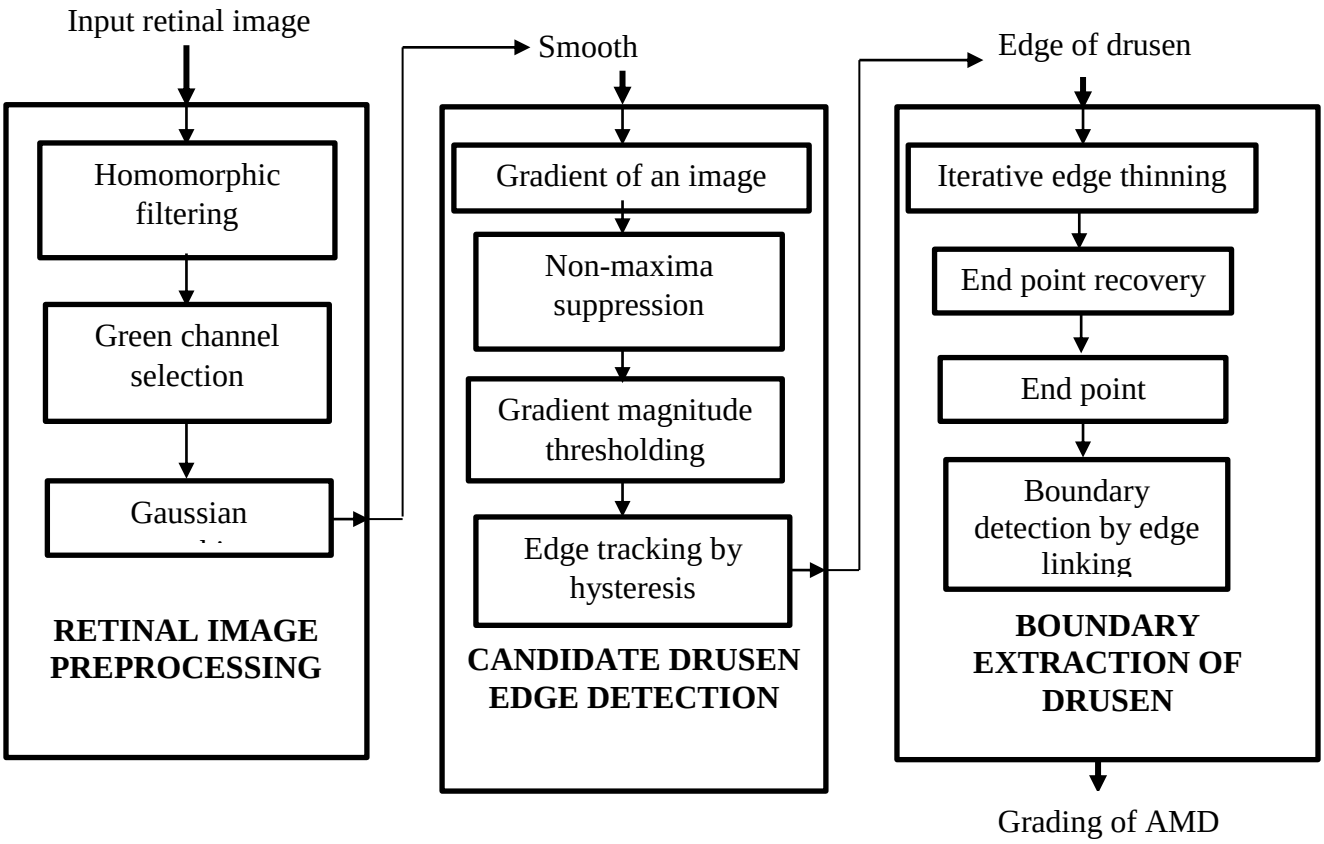

4.2: Flow chart of automated drusen detection by method 2

4.2.1 Retinal image preprocessing

The purpose of retinal image preprocessing is to remove artifacts that occur during retinal image acquisition process. One of it is non-uniform illumination which is responsible for the presence of intensity homogeneities and the shading artifacts in an

image. In addition, camera dependent factors like pixel noise and compression artifacts further degrade the image. Noise in the image may be amplified during contrast enhancement and impart a visible graininess to the image. This is highly undesirable especially in cases where the lesion characteristics are comparable to those of the artifacts produced due to noise amplification. Hence, retinal image preprocessing is done to improve the contrast and quality of an image for easy detection of lesions. Preprocessing steps are follows as: (i) green channel selection, (ii) correction of non-uniform illumination, (iii) noise removal by Gaussian filter.

a) Homomorphic filtering

Retinal images are acquired by a digital fundus camera capturing the intensity of light reflected from the retinal surface. Several patient dependent and camera dependent factors such as the retina convex surface, the lower macula reflectance in comparison to other parts of the retina, insufficient pupil dilation, poor patient collaboration and ocular media opacities i.e. cataract etc. add non-uniform illumination in the image [64]. This effect of illumination across an image contributes to variation in color and therefore different contrast among different regions present in the same image. Therefore, homomorphic filtering is used to normalize the image background to have uniform illumination. Homomorphic filtering also enhances the image by brightness range compression and contrast enhancement simultaneously [65].This approach considers an image as a function of the product of the illumination and reflectance which is represented as:-

$$g(x,y) \approx i(x,y).r(x,y) \tag{4.12}$$

where $g(x,y)$, $i(x,y)$,$r(x,y)$ represents the image intensity sensed by camera, illumination multiplicative factor and reflectance respectively and (x,y) are the Cartesian coordinate of the image.Illumination varies smoothly throughout the image therefore generating low frequency in the Fourier transform of image. On the other hand reflectance is associated with high frequency component of the image. Homomorphic filtering separates both factor by taking the logarithm on both sides as shown in Eq. (4.13) and then transform this to Fourier domain as given in Eq. (4.14).

$$\ln\{g(x,y)\} = \ln\{i(x,y)\} + \ln\{r(x,y)\} \tag{4.13}$$

$$\Im[ln\{g(x,y)\} = \Im[ln\{i(x,y)\} + \Im[ln\{r(x,y)\} = F_i(u,v) + F_r(u,v) \tag{4.14}$$

where$F_i(u,v)$ and $F_r(u,v)$ are the Fourier transforms of $\ln\{i\,(x,y)\}$ and $\ln\{r\,(x,y)\}$ respectively. Transformed image is now passed through a modified Butterworth high pass filter $H(u,v)$ in frequency domain. Modified Butterworth filter is suitable for homomorphic filtering by providing a steeper slope as well as adjusting the transition of the filter response [66] as given in Eq. (4.15).

$$H(u,v) = 1 - \frac{1}{1+(u^2+v^2/a)^n} \tag{4.15}$$

where$\frac{u^2+v^2}{a}$ determines the steepness of transition slope. Hence a filtered image$G(u,v)$ is obtained as presented in Eq. (4.16), where $F_i(u,v)$ and $F_r(u,v)$ are the Fourier transforms of $\ln\{i\,(x,y)\}$ and $\ln\{r\,(x,y)\}$ respectively.

$$G(u,v) = \{H(u,v)F_i(u,v)\} + \{H(u,v)F_r(u,v)\} \tag{4.16}$$

The spatial domain representation of filtered image is obtained by taking inverse Fourier transform of $G(u,v)$ as shown in Eq. (4.17).

$$g_{HF}(x,y) = \Im^{-1}\{g(u,v)\} \tag{4.17}$$

After that $g_{HF}(x,y)$ is enhanced by boosting the higher frequency values relative to low frequency values and an enhanced image $g_E(x,y)$ is obtained.

b) Green channel selection

The processed color retinal fundus image $g_E(x,y)$ consists three channels; green, red, and blue. Out of them, green channel is selected which is more informative and have better contrast than the rest two.

c) Gaussian filter

As explained earlier, noise at the pixel level is a major problem as it gets amplified during contrast enhancement operation. This noise has Gaussian distribution which necessitates an image smoothing operation. Therefore for the removal of noise two dimensional Gaussian filter is applied as expressed in Eq. (4.18).

$$g_F(x,y) = \frac{1}{2\pi\sigma^3} e^{-(x^2+y^2/2\sigma^2)} \tag{4.18}$$

Where $g_F(x,y)$ is Gaussian operator and σ isthe standard deviation of the Gaussian function which controls the degree of smoothening. Smooth image $g_{GF}(x,y)$, as represented in Eq. (4.19), is obtained afterwards by the application of Gaussian filter.

$$g_{GF}(x,y) = g_{HF}(x,y) \otimes g_F(x,y) \tag{4.19}$$

4.2.2 Candidate drusen edge detection

Detection of the edges of drusen plays an important role in tracing the boundary of drusen therefore following steps are carried out for edge detection of candidate drusen [67].

a) Gradient of an image

Smoothed image $g_{GF}(x,y)$ is then filtered with a sobel kernel in both horizontal and vertical direction to get first derivative of the image intensity in horizontal direction (G_x) and vertical direction (G_y). From these two images, an edge gradient in terms of its magnitude, $g_f(x,y)$, and direction$\theta(x,y)$at each pixels are found as follows.

$$\nabla g_{GF} = \begin{bmatrix} G_x \\ G_y \end{bmatrix} = \begin{bmatrix} \frac{\partial g_{GF}}{\partial x} \\ \frac{\partial g_{GF}}{\partial y} \end{bmatrix} \tag{4.20}$$

$$g_f(x,y) = \sqrt{G_x^2(x,y) + G_y^2}(x,y) \tag{4.21}$$

$$\theta(x,y) = tan^{-1}\left(\frac{G_y}{G_x}\right) \tag{4.22}$$

b) Non-maxima suppression

After getting gradient magnitude and direction, a full scan of image is done to remove unwanted pixels which may not constitute the edge. For this purpose every pixel is checked if it is a local maximum in its neighborhood in the direction of gradient or not. This can be accomplished in the following three steps:-

Step 1 - Search in the gradient direction θ to nearest45°, by using 8-connected neighborhood.

Step 2 - Compare the edge strength of the current pixel with the edge strength of the pixel in the positive and negative gradient direction.

Step 3 - If the edge strength of current pixel is largest, preserve the value of the edge strength. If not, suppress the value.

c) Gradient magnitude thresholding

This stage decides which edges are really edges and which are not. This is done by thresholding the gradient magnitude of an image. Hence two threshold values are set to clarify the different types of edge pixels. One is called high threshold value and other is called the low threshold value. If the gradient magnitude of edge pixels is higher than the high threshold value, they are marked as strong edge pixels. If the gradient magnitude of edge pixels is smaller than the high threshold value and larger than the low threshold value, they are marked as weak edge pixels. If the pixel value is smaller than the low threshold value they will be suppressed as defined in Eq. (4.23).

$$T = \begin{cases} \|\nabla g_{GF}(x,y)\| \geq t_1 & definitely\ an\ edge \\ \|\nabla g_{GF}(x,y)\| < t_1 & may\ be\ an\ edge, depend\ on\ context \\ \|\nabla g_{GF}(x,y)\| < t_0 & definitely\ not\ an\ edge \end{cases} \quad (4.23)$$

Hence, the edge obtained after thresholding is represented as:-

$$E(x,y) = \begin{cases} 1, & if\ \|\nabla f(x,y)\| > T\ for\ some\ threshold\ T \\ 0, & otherwise \end{cases} \quad (4.24)$$

where$\{(x,y): E(x,y) = 1\}$ the set of edge pixels.

4.2.3 Edge tracking by hysteresis

After thresholding, the strong edge pixels involved in the final edge image, as they are extracted from the true edges in the image but in case of weak edge pixels, these pixels can either is extracted from the true edge, or the noise/color variation. To achieve

an accurate result, weak edges may be removed, based on connectivity. If they are connected to sure edge pixels they are considered to be part of edges otherwise discarded.

a) Boundary extraction of drusen

The candidate drusen edge detection phase extracts edge of all regions which may be considered as possible drusen edge so that not a single region containing drusen should be missed at that stage. Now this stage will cater only true edges for boundary which consists of following stages.

b) Iterative edge thinning

To remove the unnecessary edge responses, edge thinning is done which comprises following steps:

Step1 – In the first step, image containing edges is converted into binary by global thresholding.

Step 2 – To remove the isolated pixels morphological thinning algorithm is applied, as given in Eq. (4.25).

$$E(x,y) \ominus S = E(x,y) - (E(x,y) \otimes S) \tag{4.25}$$

Here S is the L – type structuring element, $\ominus$ denotes the thinning operation and $\otimes$ defines the hit or miss transformation.

c) End point recovery

End point recovery, the second stage of boundary detection, examines every pixel in a top-left to bottom-left direction until an end point or junction is not encounter. For assessing the end points, edge links are scanned in eight possible directions by using a 3x3 mask as shown below. Here the pixel under investigation is highlighted and mask entries indicated by ‘x’ can take any value (0 or 1) but at least one of them has a value 1 for end point recovery.

$$\begin{bmatrix} x & x & x \\ 0 & 1 & 0 \\ 0 & 0 & 0 \end{bmatrix} \quad \begin{bmatrix} 0 & 0 & x \\ 0 & 1 & x \\ 0 & 0 & x \end{bmatrix} \quad \begin{bmatrix} 0 & 0 & 0 \\ 0 & 1 & 0 \\ x & x & x \end{bmatrix} \quad \begin{bmatrix} x & 0 & 0 \\ x & 1 & 0 \\ x & 0 & 0 \end{bmatrix}$$

d) End point labeling

The labeling of an image is a procedure designed to group, pixels with similar features and, usually adjacent pixels by assigning them common label. Hence end point labeling is done to mark the connected components. After finding the endpoints a label is assign to the pixels that are not marked. The label is then propagated to the pixel pointed out by the gradient angle and will continued to be propagated until the next one is already marked or is outside the image boundary.

4.2.4 Boundary detection by edge linking

This is used to track all the edge points starting from an end point or junction. As it tracks, it stores the coordinates of the edge points in an array and labels the pixels in the edge image with the negative of their edge number. This continues until no more connected points are found, or a junction point is encountered. It applies a local processing because in global processing i.e. Hough transform don't need to connect the edge pixels because they try to find the best fit of a known shape to the edge data [68]. Algorithm followed in local processing is as follows:

Step 1 - Analyze each pixels in small neighborhood of each edge point.

Step 2 - pixels that are similar are linked.

Step 3 - Principal properties used for establishing similarity are discussed in section 4.2.1.

a) Edge pixels with coordinates $(x_{0,}y_0)$ in the neighborhood of (x, y) is similar in magnitude to pixel at (x, y) if

$$\left|\nabla f(x, y) - \nabla f(x_{0,}y_0)\right| \leq E \tag{4.26}$$

where E is the limit of pixel for edge as discussed in Eq. (6.26).

b) Edge pixel with coordinates $(x_{0,}y_0)$ in neighborhood of (x, y) has an angle similar to pixel at (x, y) if

c) $|\alpha(x, y) - \alpha(x_0, y_0)| < A$ (4.27)

where A is the threshold for angle selection.

c) Edge pixel $(x_{0,}y_0)$ is linked with (x, y) if both criteria are satisfied.

Edge pixels are linked by examining each pixel neighbor pair and seeing if they have similar properties as given in Eq. (4.26) and (4.27). Once the links established, linked pixels are used as boundary of detected drusen.

Chapter – 5

PERFORMANCE EVALUATION

This chapter describes different types of performance parameters which are used for testing and validation of results.

5.1 EVALUATING PARAMETERS

This chapter is dedicated to validate the proposed methodologies for drusen detection and quantification. The current standard method for drusen measurement is the Wisconsin Grading System. It categorizes drusen based on size and visibility of the boundary of the biggest drusen found, and is adopted in this work. This method is done manually by trained specialists due to lack of automatic and reliable quantification tools hence an automatic method is employed in the proposed methodology.

The validation of results of the automatic methodology for drusen detection is done by comparing it with ground truth. To create ground truth i.e. reference set of images, images are marked manually which is used to evaluate the agreement with the automated method. To mark these images for ground truth, stylus is used to draw the boundary of drusen on ipad.

The manual segmentation and measurement of Drusen are quite difficult, time consuming, and the user may make mistakes also. The results of the segmentation can vary depending on the image quality and experience of user. Hence for this application certain standard parameters are used to evaluate the segmentation performances by matching pixel-to-pixel values of manual and automated detected drusen. The accuracy of the proposed automated quantification of drusen is assessed by detecting the affected area of drusen. In this work these parameters like sensitivity, specificity, accuracy, positive predictive value and Matthew's correlation coefficient are assessed by using publicly available datasets.

Database is a tool for evaluation and comparisons of different algorithms. In order to evaluate algorithms for automated screening and diagnosis of retinal disease, some of the benchmark databases are publicly available. The purpose of these databases is to check the validity of systems and to compare the results with the existing techniques. In

this paper, two databases named STARE (Structured Analysis of Retina) and ARIA (Automated Retinal Image Analysis) are used to check the validity of systems and to compare the results with the existing methods.

The STARE database is acquired using TOPCON fundus camera with 35 degree field of view and a resolution of 700x605 pixels. It consists of total 400 images form which 36 is for normal AMD and 48 for AMD images [69].

The ARIA database is acquired using Carl Zeiss Meditec fundus camera with 50 degree field of view and a resolution of 768x576 pixels. It consists of 101 normal and 11 AMD images as described in Table 2 [70]. Out of 59 AMD images from STARE and ARIA database 48 images (37 from STARE and 11 from ARIA) are used for validation of results.

When a pixel is classified as drusen in both the ground state and segmented state it is known **as true positive.** When a pixel is classified as a non drusen in the ground truth and segmented image it can be defined **as true negative.** In **false negative** a pixel is classified as non drusen in the segmented image but as a drusen pixel in the ground truth image**.** When a pixel is marked as drusen in the segmented image but non drusen in the ground truth image it is known as **false positive.** Some other parameters are used to present the results in more understandable form. They are sensitivity, specificity, accuracy, positive predictive value (PPV) and Matthew's correlation coefficient (MCC).

Sensitivity– Sensitivity of the proposed method is the ability to identify drusen pixels correctly. Mathematically it can be expressed as:

$$\text{Sensitivity} = \frac{T_P}{(T_P+T_N)} \tag{5.1}$$

Specificity–Specificity of the proposed method is the ability to identify non-drusen pixels correctly. Mathematically it can be expressed as:

$$\text{Specificity} = \frac{T_N}{(T_N+F_P)} \tag{5.2}$$

Accuracy –Accuracy of the proposed method is the proportion of true results in terms of correct drusen pixels and non-drusen pixels among the total number of pixels examined. Mathematically it can be expressed as:

$$\text{Accuracy} = \frac{(T_N+T_P)}{(T_N+T_P+F_N+F_P)} \tag{5.3}$$

Positive predictive value (PPV) – It is the probability to detect correct drusen pixels out of all detected drusen pixels by the method. Mathematically can be expressed as:

$$\text{PPV} = \frac{T_P}{(T_P+F_P)} \tag{5.4}$$

Matthew's correlation coefficient (MCC) – MCC is a measure to evaluate the method by measuring the correlation coefficient of the ground truth and detected drusen by the proposed method.

$$\text{MCC} = \frac{T_N*T_P-F_N*F_P}{\sqrt{(T_P+F_P)(T_P+F_N)(T_N+F_P)(T_N+F_N)}} \tag{5.5}$$

Here T_P are true positive means drusen regions correctly classified.T_N, are true negative means non drusen regions correctly classified. F_P, ar false positives means non drusen regions wrongly classified as drusen regions. F_N, are false negatives means drusen regions wrongly classified as non drusen regions.

5.2 Grading of AMD [71]

Retinal color fundus imaging has been widely used for AMD grading. A number of grading protocols has been established for drusen grading which helps in identifying the stage of AMD using color fundus imaging. Among these protocols Wisconsin Age-related Maculopathy Grading system, the International Classification and Grading System for Age-related Maculopathy and Age-related Macular Degeneration and its modified version are widely used. These methods mainly use computer software tools that a grader uses to manually count the drusen through drawing different sizes of circles in the software interface. The quantification of drusen and grading of AMD using manual methods over fundus photographs is not commonly used as it is a fastidious process and lacks reproducibility. Also, the variability within the analyses performed by different ophthalmologists limits the use of this technique. Hence, automated AMD grading

techniques are used for the diagnosis of disease severity level. There are a number of articles have been published on drusen quantification using retinal fundus imaging but out of these only a few of them are utilized drusen size, area and actual number in the image to grade the AMD severity as explained in the literature review section as well as only a few of techniques can classify into small, intermediate and soft. Most of these automatic techniques are constrained in determining the drusen segmentation level and absence and presence of drusen in the retina.

In this paper, an automatic, accurate and efficient classification and quantification of drusen with considering drusen position, size, shape, area and actual number of drusen present in retinal fundus images can provide a useful tool to define the severity of AMD. Use of such tool would help to determine the severity of risk for progressive sight threatening advanced AMD. AREDS grading system defines the AMD category as 1 to 4 - normal to severe AMD based on the drusen, geography atrophy, retinal pigment epithelium and neovascularization following Wisconsin grading protocol which is applied in this paper. The study defines AMD category as 1 if there is no drusen exists or drusen size < 63 μm and total area covered by drusen is < 125 μm. AMD category 2 or intermediate is defined as drusen size $\geq$ 63 μm and < 125 μm and drusen area $\geq$ 125 μm but GA absent. AMD category 3a is defined as intermediate $\geq$ 63 μm and < 125 μm, drusen area 360 μm diameter circle if soft distinct drusen are present and $\geq$ 656 μm diameter circle if soft indistinct drusen are present as illustrated in Table 5.1.

Performance of grading done by proposed method is also evaluated by comparing it with ground truth grading in terms of non-overlapping drusen area, size and number of drusen.

Non-overlapped drusen area – To measure the non-overlapped area, comparison of segmented drusen by proposed method and same with ground truth is done. Here comparison is done pixel-by-pixel to find the true size and area of drusen.

Numbers of drusen – To measure the accuracy of drusen types thirty four images are selected which includes small, intermediate and soft or large drusen. Afterwards, numbers of each drusen type in the individual images are counted for both manually

measured and automatically detected. Here accuracy is computed in percentage for different drusen types and also compared with other existing methods.

Table 5.1: AREDS grading system

AMD Category	**Types of drusen**	**Drusen size**	**Drusen Area**	**Number of drusen**	**Pigment abnormalities**
1	None or small	$< 63\ \mu m$	$< 125\ \mu m$ diameter circle	≈5-15 small drusen	None
2	Small Or Intermediate	$< 63\ \mu m$ or $\geq 63, >125\ \mu m$ Doesn't matter if pigment abnormalities present.	$\geq 125\ \mu m$ diameter circle.	Not specified At least one intermediate drusen should present	Absent or present, but GA absent
3a	Intermediate Or Large	$\geq, <125\ \mu m$ or $\geq 125\ \mu m$ None required if non-central GA present.	$\geq 360\ \mu m$ diameter circle if soft indistinct drusen are present $\geq 656 \mu m$ Diameter circle if soft indistinct drusen are absent.	> 20 drusen At least one large drusen should present	Absent or present but GA absent

Chapter – 6

RESULTS AND DISCUSSION

This chapter will discuss the results and discussion of automated method 1 and method 2 respectively, discussed below.

6.1 Method 1

6.1.1 Green channel selection

This algorithm is tested on 36 images, publically available datasets i.e. STARE and ARIA, acquired by the Fundus camera as shown in Fig. 6.1 (a). It is observed from the Fig. 6.1 (b) and (c) that the green channel is selected for further processing because it having better contrast than the other channels.

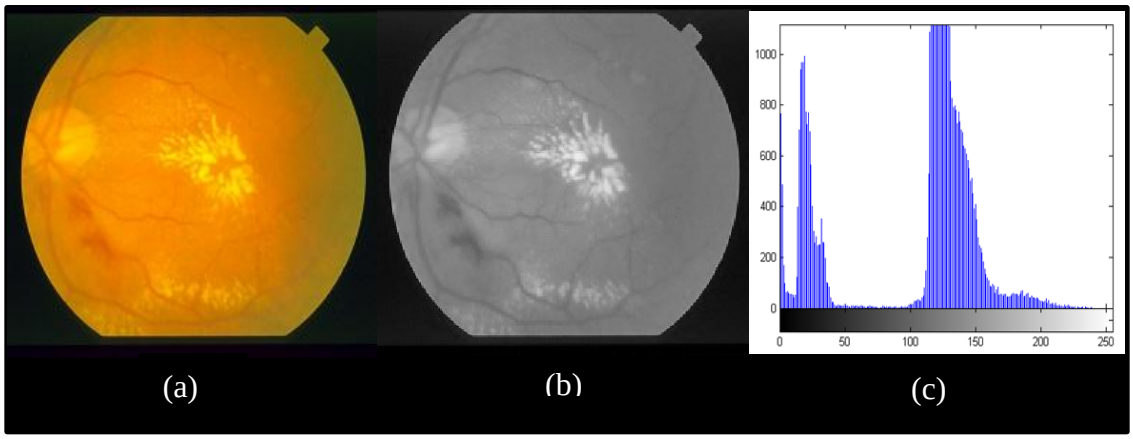

Figure 6.1: Green channel selection; (a) color retinal fundus image from STARE dataset; (b) green Channel of fundus image; (c) histogram of green channel having better contrast

6.1.2 Non-uniform illumination correction

Central part of the retina is focused by defining a rectangle at the right or left side of the optical nerve (right or left eye, respectively). Fig. 6.2 (a) presents example of gray-scale version (green band) of the original color image. Drusen show up as bright blobs, but automatic extraction of these pathological features is difficult, since drusen vary in shape and size and tend to spread (varying brightness) around their location. Additionally, small bright regions of the background tend to create larger than can be mistaken as large drusen hence to remove such type of false negative, an approximation

of background as a separate image is considered by using morphological operation. A surface plot of background is shown in Fig. 6.2 (b) to visualize the variation of background. After subtracting this approximated image from the original image a uniform image is obtained as shown in Fig 6.2 (c), which shows the variation in drusen and background.

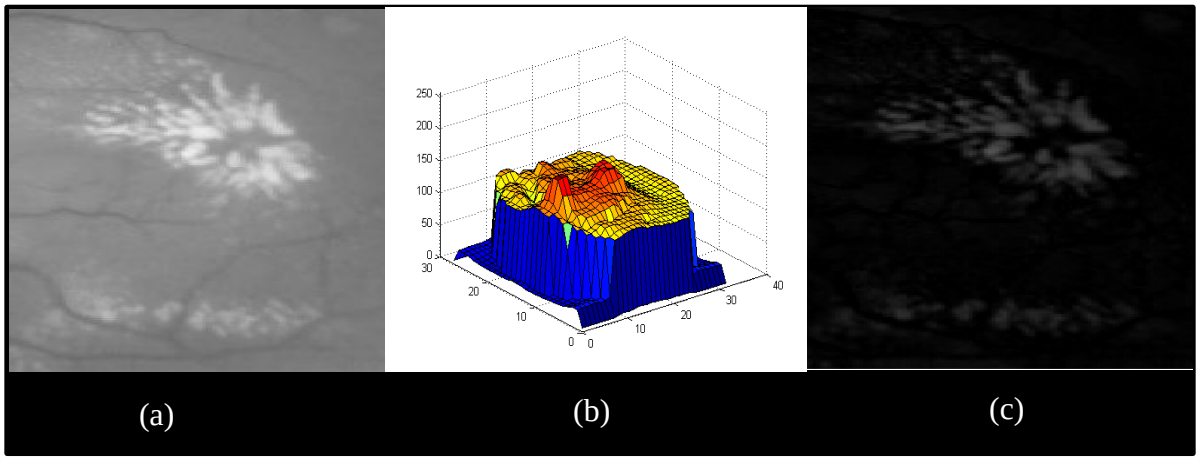

Figure 6.2: Result of non-uniform illumination and contrast enhancement; (d) test image from Original gray image; (e) surface plot of approximated background; (f) image with uniform illumination after subtracting approximated image from original image

6.1.3 Contrast enhancement

Contrast of an image has been enhanced by using automated contrast enhancement technique which enhanced the local intensity globally as shown in Fig. 6.3 (a).

6.1.4 Drusen detection

Segmentation of an image is done by Otsu' threshold which ideally locate candidate region of drusen and with the help of morphological operation noise can be removed as shown in Fig. 6.4 (b). There are no vague results found. Pseudo color indexed image is used for visualization of no. of drusen present in retinal fundus images as shown in Fig. 6.3 (c).

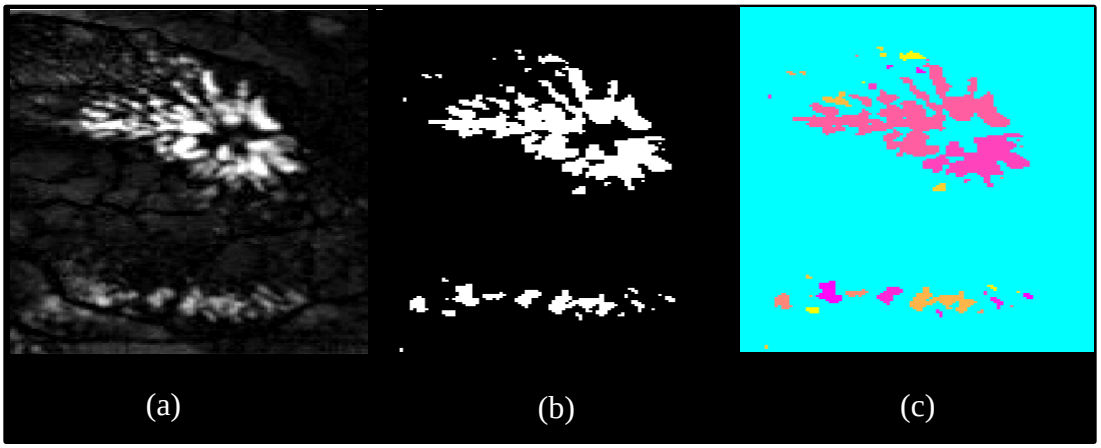

Figure 6.3: Result of segmentation; (a) enhanced image; (b) binarization of image using Otsu's thresholding; (c) Pseudo color indexed image

6.1.5 Pixel-wise feature extraction

Pixel-wise feature extraction is done in binarized image to identify the total number of drusen present in image. As drusen varies in its shape and size which may be overlapped on each other. Therefore pixel-wise feature extraction is used because which is based on calculation of weighted centroid and standard deviation of individual pixels. As in Fig. 6.4 (a) and (b), weighted centroid and standard deviation of individual components can be visualized by above mentioned Eq. (10, 11). Graph shows in Fig. 6.4 (d) the regional maximum intensity with respect to standard deviation which shows the intensity of individual components.

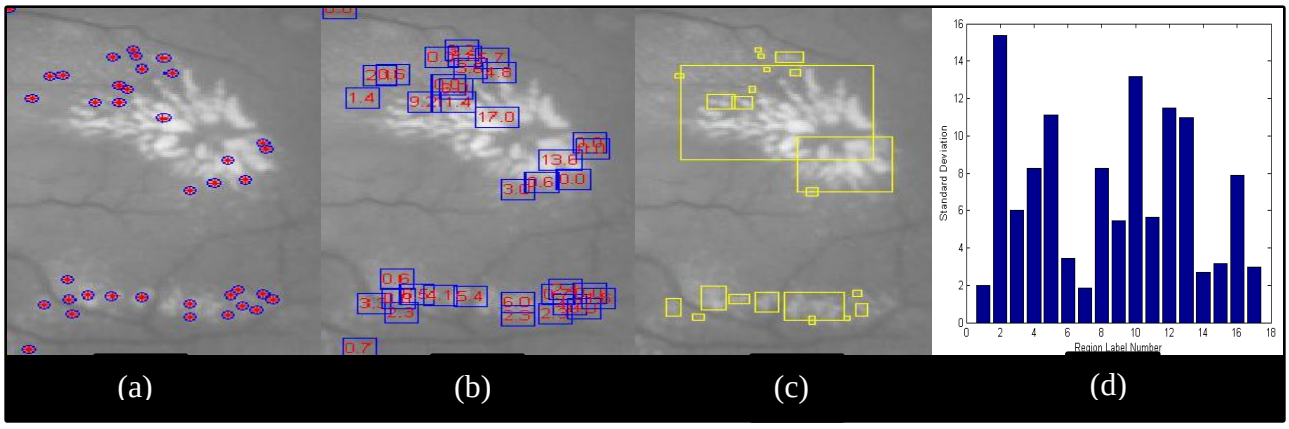

Figure 6.4: Results of drusen detection, (a) weighted centroid of components, (b) standard deviation of objects in image, (c) components with standard deviation>2, (d) regional label no. w.r.t standard deviation

6.1.6 Edge detection of drusen

Canny edge detector is used to detect the edge of each individual drusen. The canny edge detector is widely used to locate the sharp intensity changes and to find object boundaries in an image. It classifies a pixel as an edge if the gradient of the pixel is larger than those of pixels at both its sides in the direction of maximum intensity change. Area is calculated by an Eq. (8) in pixels. The total area affected by drusen is in pixels. The proposed algorithm has been tested 36 images out of which results of some test images are shown in Fig. 6.5, which shows the edge of the drusen and its total area in pixels.

NAME OF IMAGES	TEST IMAGE	EDGE OF DETECTED DRUSEN	AREA IN PIXELS
Im0003	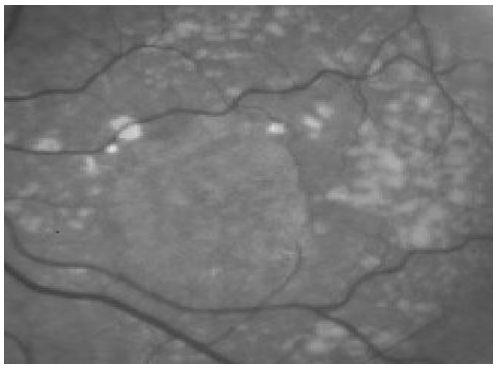	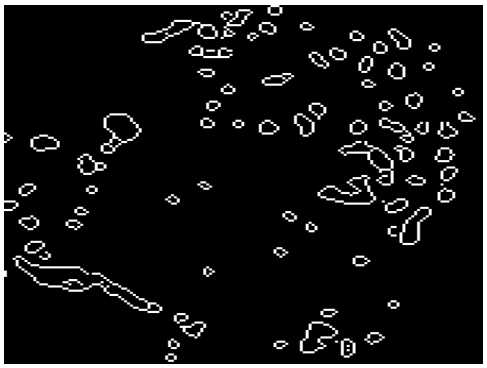	2275
Im0006	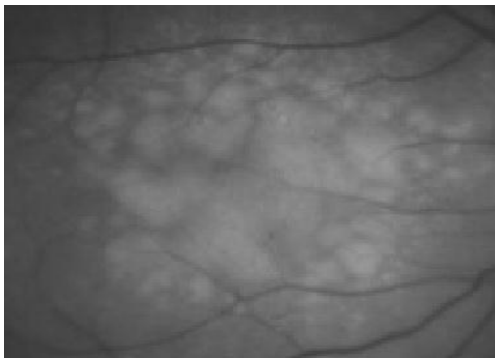		2122

Im0012	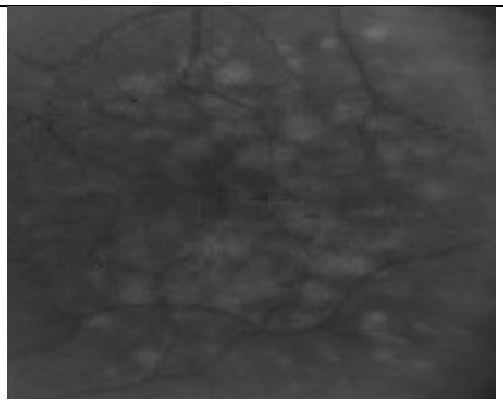	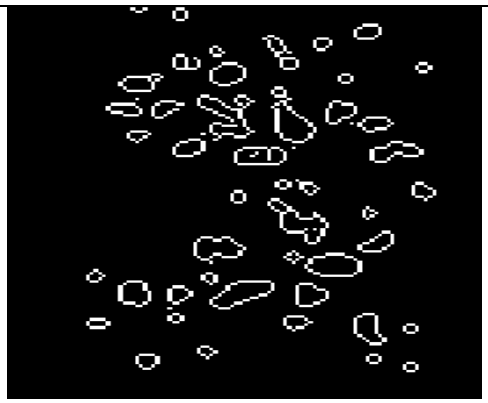	1463
Im0037	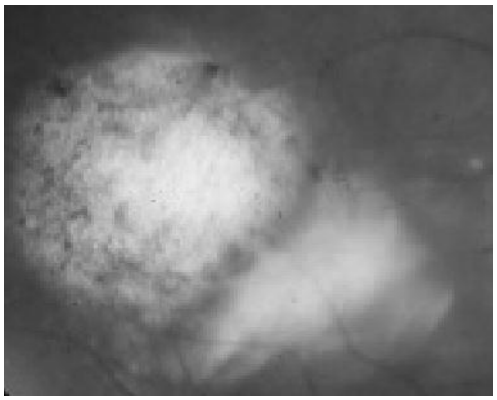	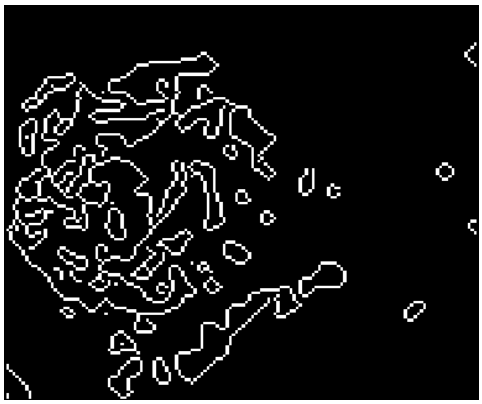	1991
Im0041	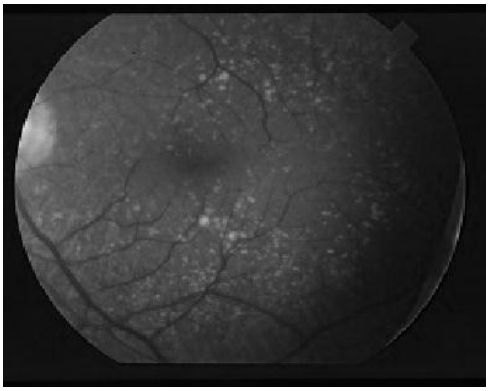	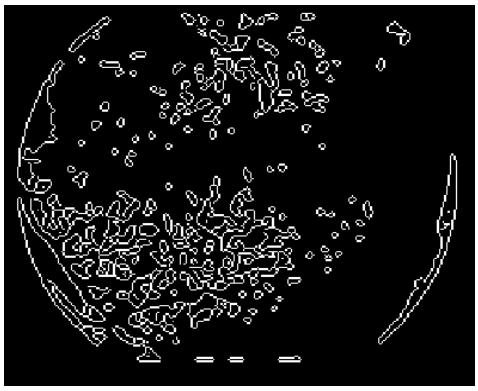	1362
Im0063	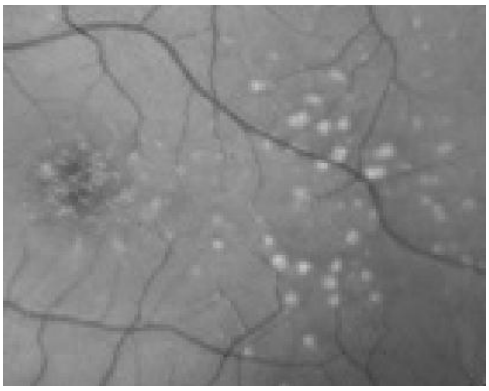	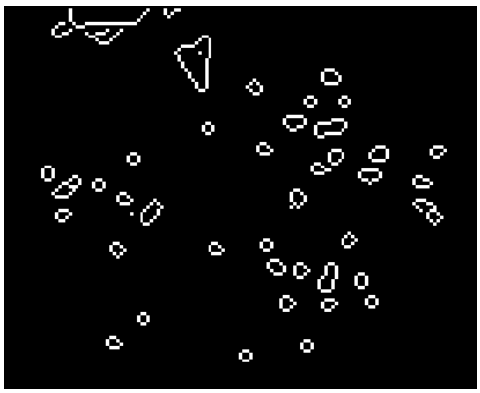	725

Im0079	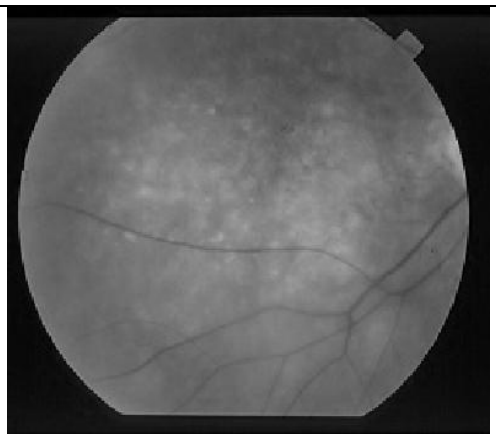	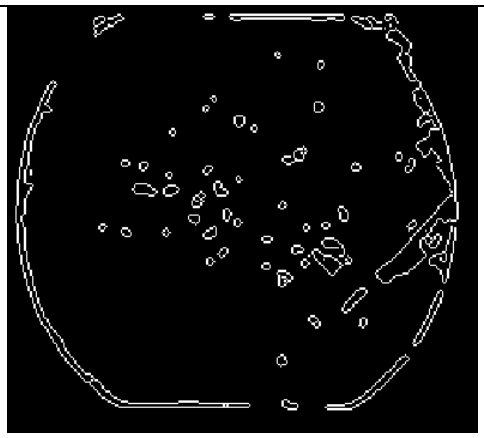	1920
Im0147	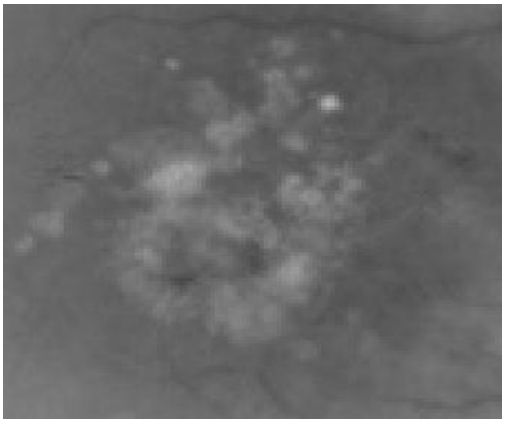	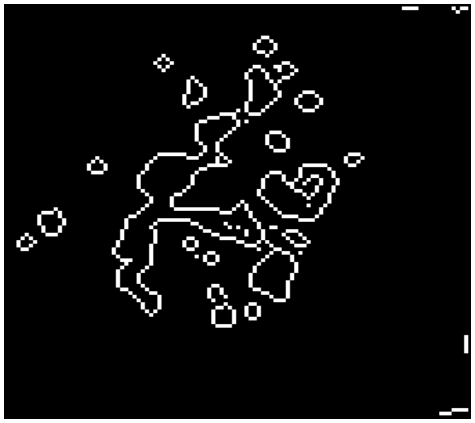	2182
Im0265	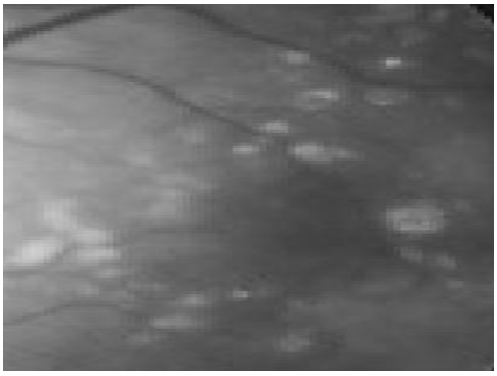	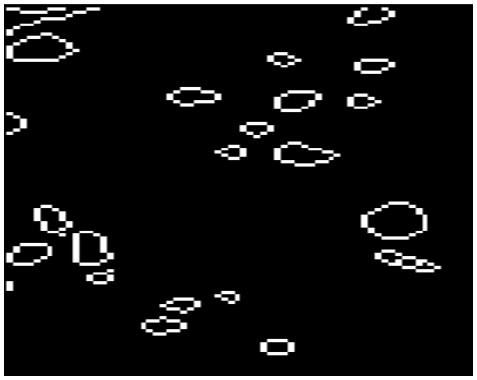	445
Im0266	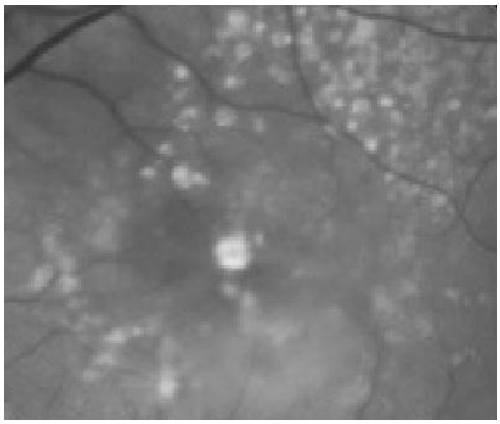	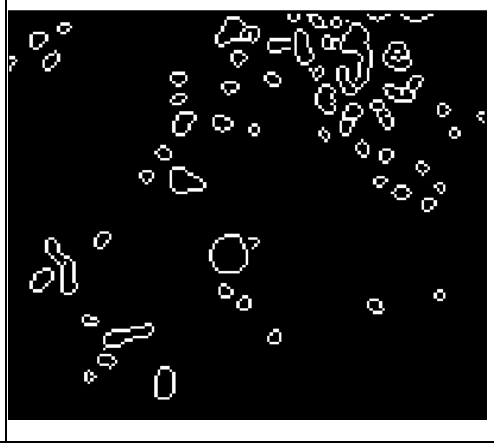	1020

Im0270	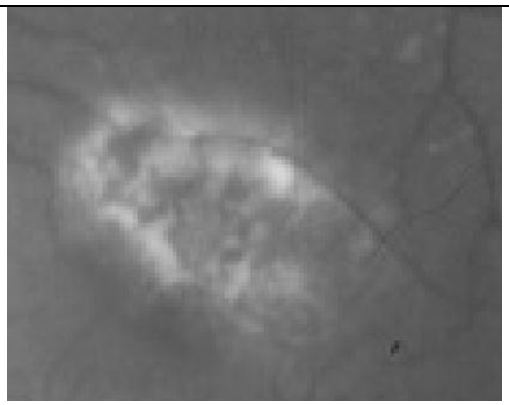		859
Im0271	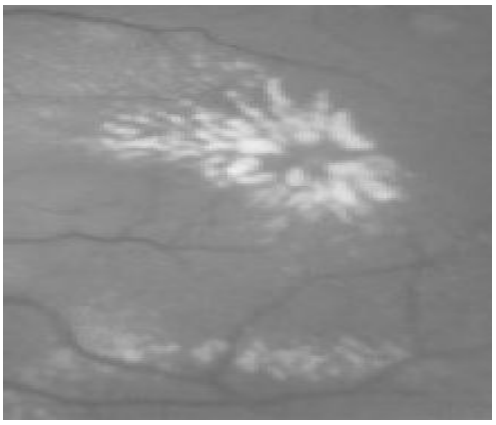		1698
Im0281	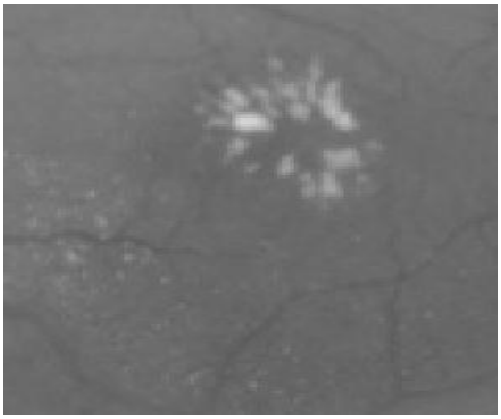	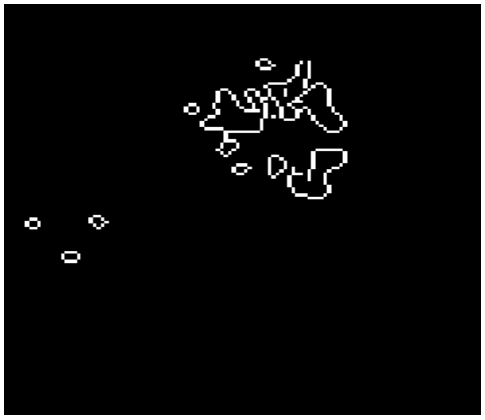	563
Im0382	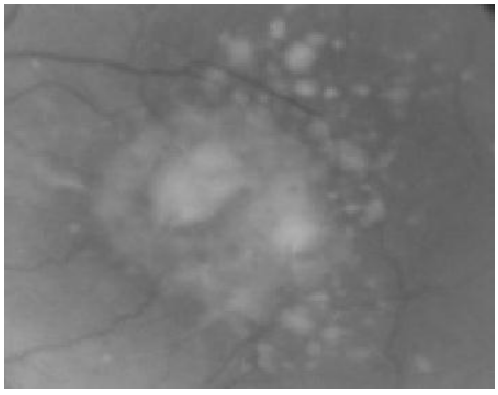	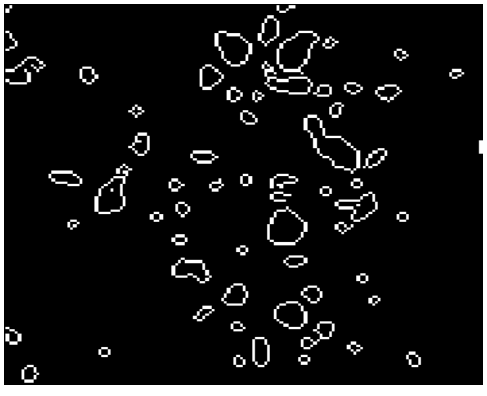	1963

Figure 6.5: Results of edge detection and quantification of drusen in retinal fundus images; column 1 showing list of images; column 2 showing test images; column 3 showing edge of detected drusen; column 4 showing area in pixel

6.1.7 Grading of AMD

After quantification of segmented drusen it is compared with the ground truth i.e. manually segmented drusen as shown in table 4. Proposed method has achieved 93.2% drusen detection accuracy, 82% sensitivity, 91.3% specificity and 92.21% PPV. After comparing results of proposed method with ground truth it can be concluded that the present system having better results with less non-overlapped drusen region ranging from 0 to 3.156 for small drusen, 0 to 14.329 for intermediate drusen and 0.72 to 19.41 for large or soft druse. It can be clearly seen from the table 6.1, the proposed method achives average accuracy of 91.8% for small drusen, 98.66% for intermediate drusen and 92.91% for large or soft drusen, outwits the results of Bhuiyan et al. [63]. The results demonstrated that the proposed system could identify all the intermediate drusen and took less time of 0.042 seconds to quantify the drusen area.

Table 6.1: Classification and Quantitative analysis of drusen to grade the severity of AMD for Method 1

	Images	**Total no. Of drusen by the ground truth**	**Total drusen area in the ground truth (μm^2)**	**Size of drusen (μm)**	**Total no. Of drusen by the proposed method**	**Total drusen area by the proposed method μm^2**	**Size of drusen in μm**	**Non-overlapped area**
SMALL	IM0013	4	73.58	46.508	4	72.85	46.508	0.00
	IM0015	12	$1.362X10^{11}$	39.627	10	$1.0035X10^{11}$	36.471	3.156
	IM0046	15	63.84685866	98.899	12	73.84675856	98.880	0.019
	IM0262	9	$2.028X10^{10}$	52.829	8	$1.997X10^{10}$	51.064	1.765

	IM0401	6	$1.317X10^{10}$	48.752	6	$1.188X10^{10}$	48.518	0.234
	IM0402	5	$1.173481523 X10^{10}$	25.975	5	$1.021730348 X10^{10}$	25.135	0.84

	Images	**Total no. Of drusen by the ground truth**	**Total drusen area in the ground truth (μm^2)**	**Size of drusen (μm)**	**Total no. Of drusen by the proposed method**	**Total drusen area by the proposed method μm^2**	**Size of drusen in μm**	**Non-overlapped area**
INTERMEDIATE	IM0006	35	$1.973X10^{11}$	72.002	33	$1.581X10^{11}$	63.446	8.556
	IM0007	18	$1.263X10^{11}$	68.271	18	$1.240X10^{11}$	68.116	0.155
	IM0012	46	$1.463X10^{11}$	74.002	43	$1.365X10^{11}$	62.436	11.566
	IM0033	87	$2.033X10^{11}$	106.111	87	$2.025X10^{11}$	104.028	2.083
	IM0038	25	$1.168X10^{10}$	67.002	25	$1.002X10^{11}$	64.363	2.639
	IM0066	50	$2.209X10^{10}$	103.981	50	$2.368X10^{10}$	95.652	14.329
	IM0068	125	$1.689X10^{10}$	63.932	125	$1.653X10^{10}$	63.500	0.432
	IM0079	40	$1.135X10^{10}$	69.842	36	$1.026X10^{11}$	69.225	0.617
	IM0097	20	$1.139X10^{10}$	127.854	20	$1.133X10^{10}$	127.854	0.0
	IM0192	136	$2.603X10^{12}$	118.295	136	$2.031X10^{12}$	118.268	0.027
	IM0263	89	$1.759X10^{10}$	72.654	89	$1.708X10^{10}$	72.652	0.002
	IM0376	2	90.985	127.541	2	90.977	127.541	0.008

	Images	**Total no. Of drusen by the ground truth**	**Total drusen area in the ground truth (μm^2)**	**Size of drusen (μm)**	**Total no. Of drusen by the proposed method**	**Total drusen area by the proposed method μm^2**	**Size of drusen in μm**	**Non-overlapped area**
LARGE or SOFT	IM0003	124	$3.782X10^{11}$	157.241	119	$3.255X10^{11}$	157.002	0.239
	IM0037	45	$2.511X10^{11}$	152.115	45	$2.156X10^{11}$	150.221	1.894
	IM0041	125	$1.984X10^{11}$	92.475	120	$1.664X10^{11}$	92.036	0.439
	IM0063	56	$3.620X10^{10}$	248.708	52	$3.160X10^{10}$	248.521	0.187
	IM0143	27	$9.484X10^{10}$	336.125	27	$9.454X10^{10}$	336.020	0.105
	IM0147	33	$3.329X10^{11}$	183.6320	33	$3.332X10^{11}$	183.613	0.019
	IM0148	41	$5.113X10^{11}$	82.366	41	$5.039X10^{11}$	82.285	0.081
	IM0265	43	$1.201X10^{10}$	176.24	40	$1.386X10^{10}$	174.625	1.615
	IM0266	98	$6.935X10^{10}$	558.68	94	$6.283X10^{10}$	539.27	19.41
	IM0267	112	$1.496X10^{10}$	669.252	106	$1.251X10^{11}$	652.395	16.857
	IM0270	10	$5.174X10^{10}$	152.231	10	$5.135X10^{10}$	152.135	0.096
	IM0271	26	$7.132X10^{10}$	119.565	26	$7.083X10^{10}$	119.327	0.238
	IM0281	31	$2.219X10^{10}$	560.013	31	$2.218X10^{10}$	556.916	3.097
	IM0288	39	$3.998X10^{11}$	146.522	36	$3.081X10^{11}$	143.366	3.156
	IM0382	82	$2.676X10^{11}$	445.22	82	$2.580X10^{11}$	444.50	0.72
	ARIA_13	96	$5.073X10^{11}$	135.236	92	$4.998X10^{11}$	132.583	2.653

6.2 Method 2

The proposed method for boundary detection of drusen is implemented in MATLAB version 7.10 on a PC with Intel core i3 (2.40GHZ) processor. The detailed evaluation testing and validation of the proposed method is carried out with 48 retinal images taken from two standard retinal image database; STARE and ARIA. Both databases have retinal images with different resolution. Out of these 48 images, 37 are from STARE database and 11 are from ARIA database. The results of the experiment are demonstrated with two example retinal fundus images as shown in Fig. 6.6 (a) and (b), where Fig. 6.6 (a) is the original image from STARE database and Fig. 6.6 (b) is the same from ARIA database.

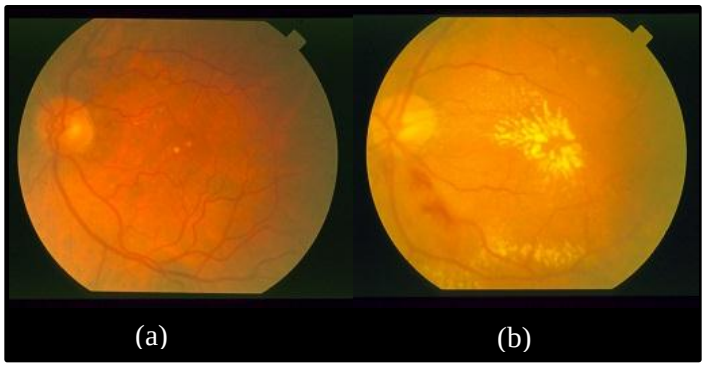

Figure 6.6: Original images from (a) STARE database (b) ARIA database

6.2.1 Preprocessing

Non-uniform illumination correction of the retinal images is performed with homomorphic filter having the best filtering results with the parameter values set as boost = 2, cut-off frequency = 0.5 and order = 2 during the experiment. The filtered images after homomorphic filtering for Fig. 6.6 (a) and (b) are shown in Fig. 6.7 (a) and (d) respectively. It can be clearly seen that the filter, designed with the above parameter settings, compresses the dynamic range of the images and enhances their contrast along with the removal of non-uniform illumination effect. Afterwards, the selection of green channel from filtered image is carried out to obtain more information in terms of better contrast. Fig. 6.7 (b) and (e) represent the selected green channel images of the filtered

images shown in Fig 6.6 (a) and (d) respectively. Furthermore, these green channel images may have pixel level noise showing Gaussian distribution. Therefore, Gaussian filter is used to remove the effect of such noise. A suitable value of σ for Gaussian filter is obtained as 1.5 with the best result of an experiment which was carried out with different values of σin the range of 1 to 2.The effect of smoothing can be clearly seen in the images 6.7 (c) and (f) after Gaussian filtering on images 6.7 (b) and (e) respectively.

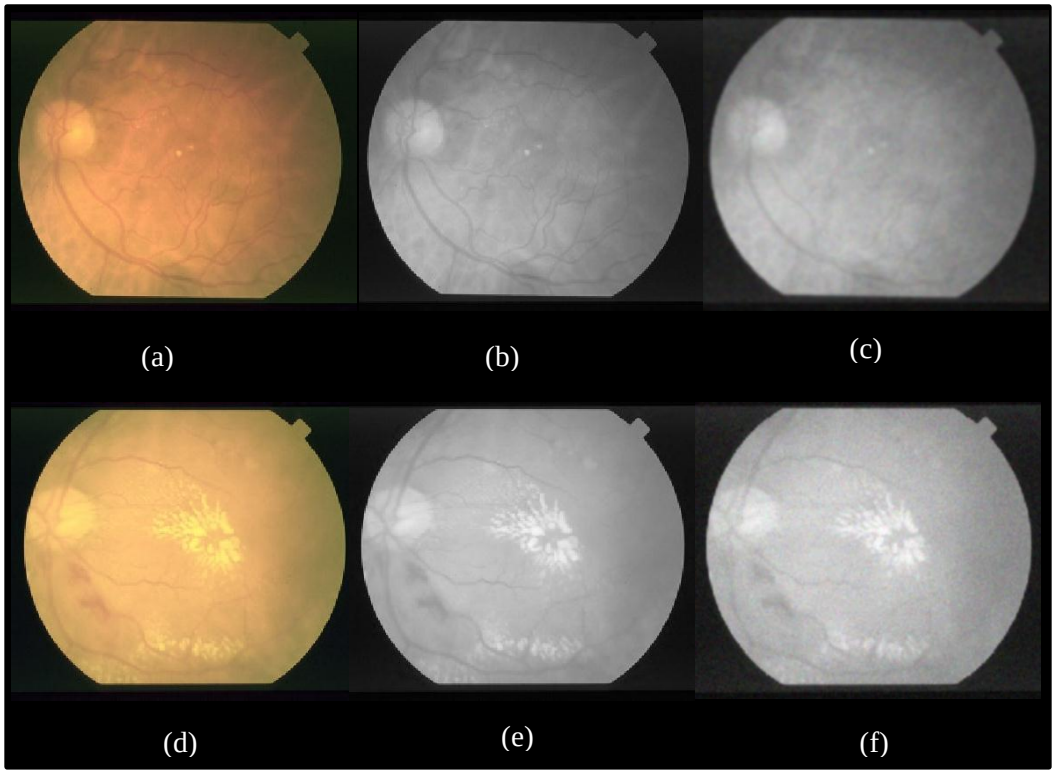

Figure 6.7: Results of preprocessing of retinal fundus images: Images (a) and (d) demonstrates the effect on image after homomorphic filtering; images (b) and (e) represents the green channel of filtered image (a) and (d) and images (c) and (f) illustrates the effect of smoothing after Gaussian filtering

6.2.2 Candidate drusen edge detection

Drusen are the brightest intensity regions (except optic disc) in a retinal fundus image and therefore at their edges have maximum change in intensity with respect to neighborhood pixels. Detection of the edges of candidate drusen is possible by finding the gradient of a retinal image obtained after preprocessing step. Gradient vector at each pixel indicates the direction of the maximum change in intensity. Drusen are bright blobs,

so gradient image will show the higher magnitude of the gradient vector at the edges of drusen in comparison to the rest gradient vectors present at other pixels of the same image. Gradient vector images, as shown in Fig. 6.8 (a) and (d) after zooming, are obtained by taking the gradient of the images, received after preprocessing steps, as shown in Fig. 6.7 (c) and (f) respectively. Fig. 6.8 (a) and (d) clearly show the highest strength of gradient vector at the edges of drusen. All local maxima in the gradient images are preserved by comparing edge strength of pixels by its neighborhood in positive and negative gradient direction. This will help in preserving the edges of drusen. Fig. 6.8 (b) and (e) show the quiver plot of images corresponding to the gradient images in fig. 6.8 (a) and (d) respectively. Drusen are highlighted by suppressing non-maxima gradient in the quiver plot of images. Therefore, two threshold value are selected i.e. maximum hysteresis thresholding =0.28, minimum hysteresis thresholding = 0.020 after number of experimental trails on the database images. These values will highlight only the strong pixels in the form of edges of drusen as shown in Fig. 6.8 (c) and (f) for the corresponding gradient images, Fig. 6.8 (a) and (d) respectively.

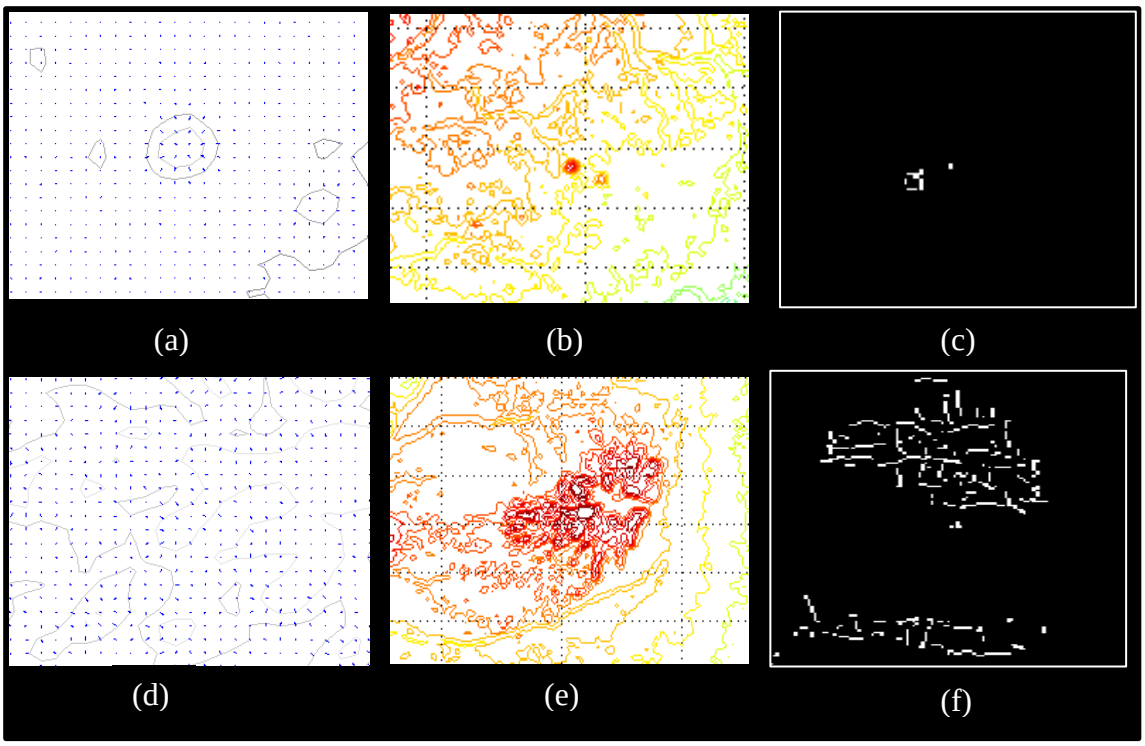

Figure 6.8: Results of candidate drusen edge detection: Images (a) and (d) represents the gradient of a smoothed image 6.7 (c) and (f); images 6.8 (b) and (e) highlights the drusen after non-maxima suppression; images 6.8 (c) and (f) represents the edge of candidate drusen

6.2.3 Boundary extraction of drusen

Edge obtained after thresholding with hysteresis have some gap in between the pixels which makes it irregular in shape. Hence, before extracting the boundary of drusen, edge should be thinned by converting it into binary form through global thresholding [23] and removing the isolated pixels with morphological thinning algorithm. After that, assessment for the edge links or junctions was performed by scanning in all possible directions. Edge links or junctions after finding are labeled to mark the connected components. The label is propagated until the next one is already marked or is outside the image boundary. Fig. 6.9 (a) and (d) show the corresponding leveled images in continuation with the previous images. Labeling is used to track all the edge pixels starting from end point or junction to find all the connected components. After finding all connected components it will link all these pixels to form a boundary of drusen as showed in Fig. 6.9 (b) and (e) respectively. Extracted boundaries of drusen are highlighted by pseudo color as shown in Fig. 6.9 (c) and (f) respectively. Pseudo color helps in counting the total number of drusen present in an image.

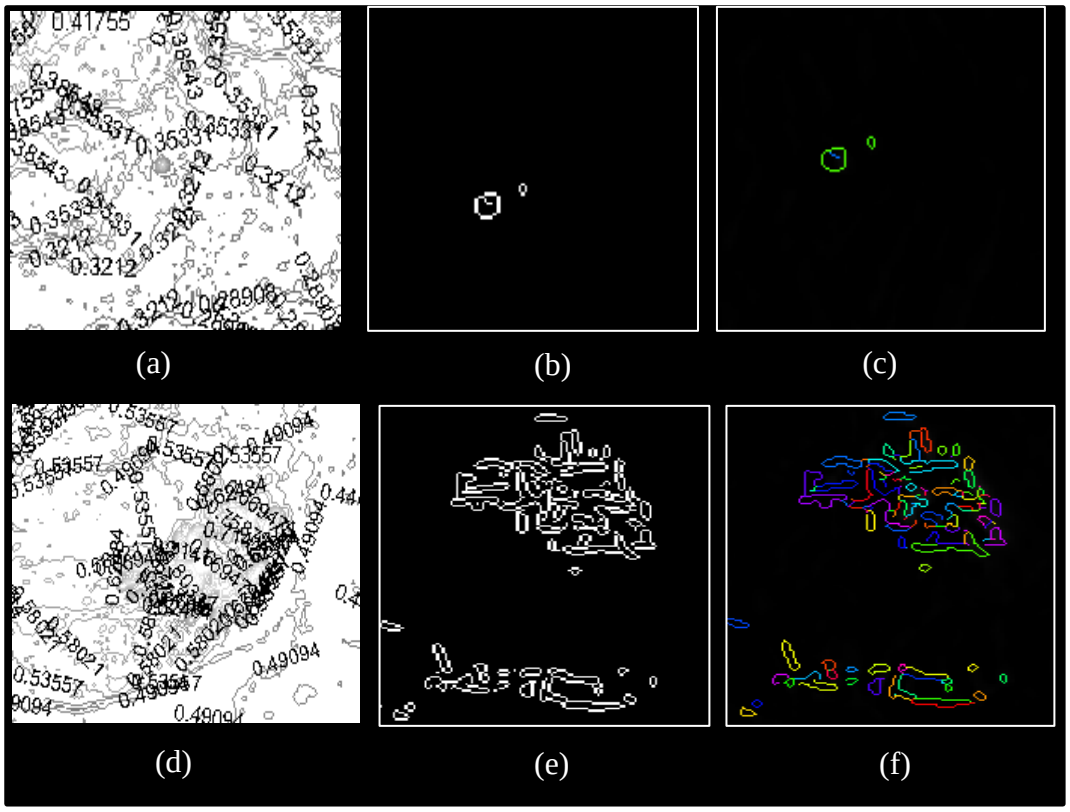

Figure 6.9: Results of boundary extraction of drusen: Images (a) and (d) depicts the labeling of an image; images (b) and (e) represents the boundary of drusen and images (c) and (f) represents the Pseudo color indexed image

NAME OF IMAGES	TEST IMAGE	EDGE OF DETECTED DRUSEN	PSEUDO COLORED IMAGES
IM0013	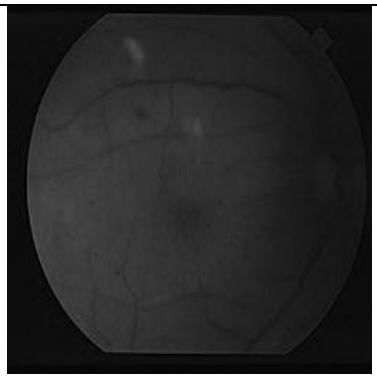	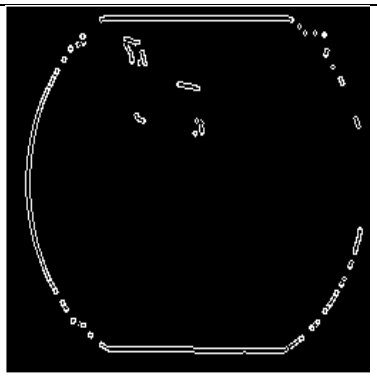	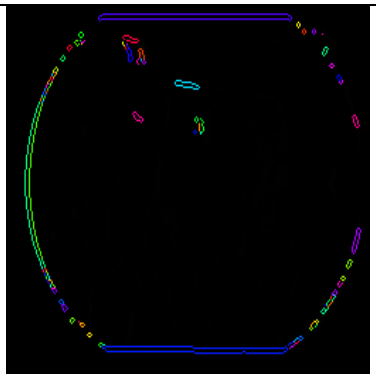
IM0062	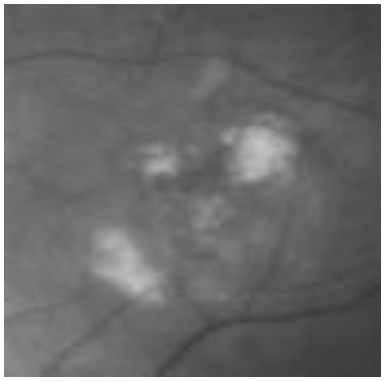	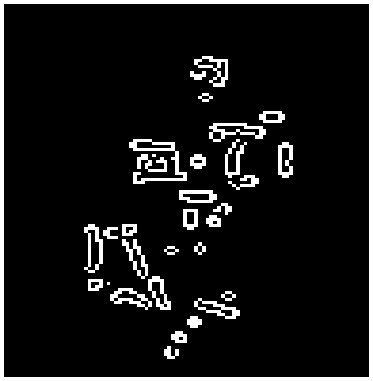	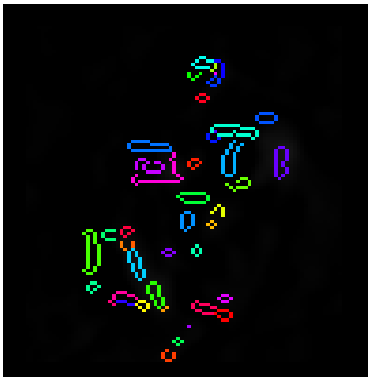
IM0175	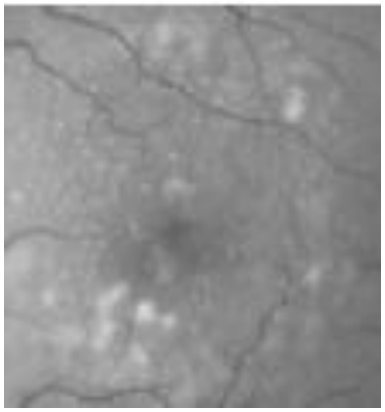	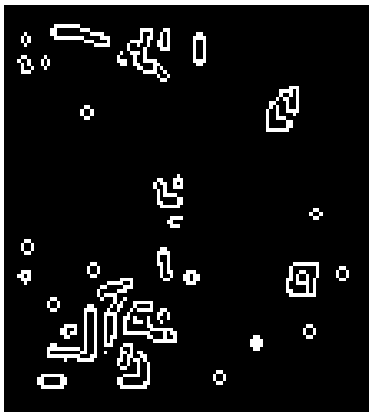	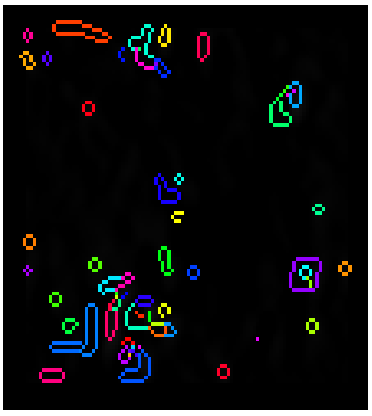

IM0206		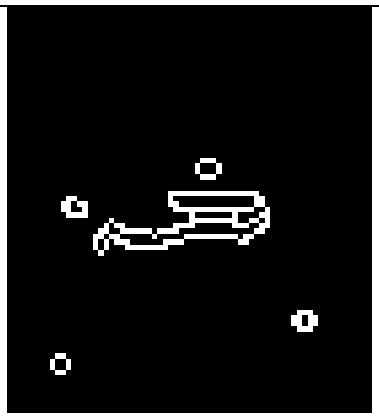	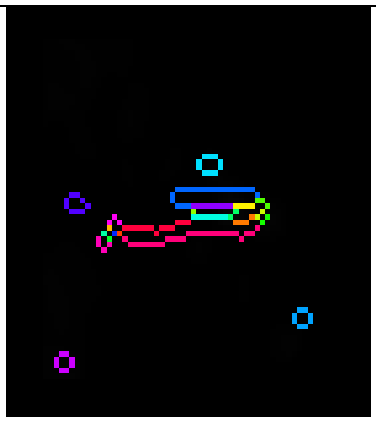
IM0259	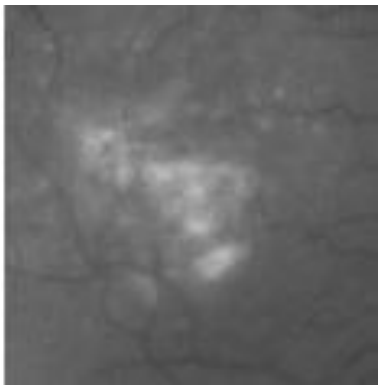	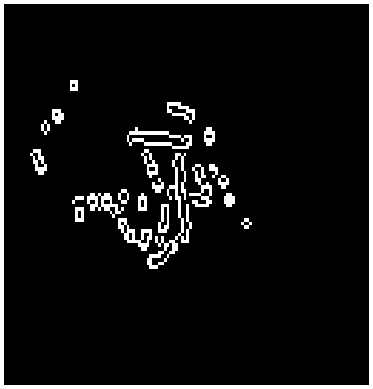	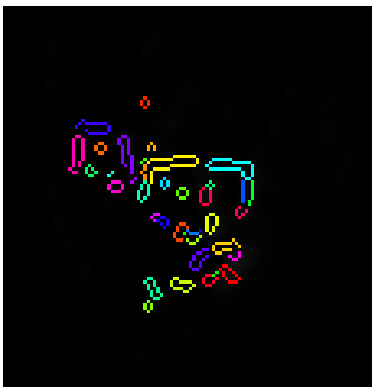
IM0269	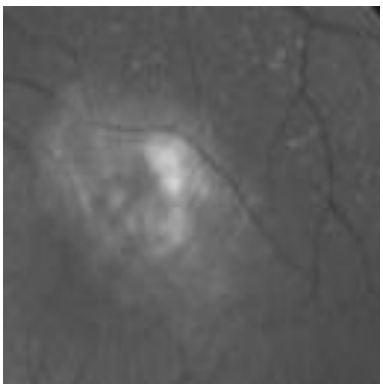	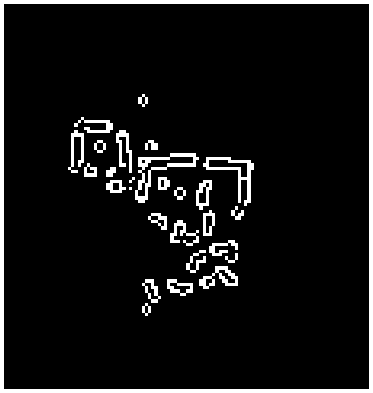	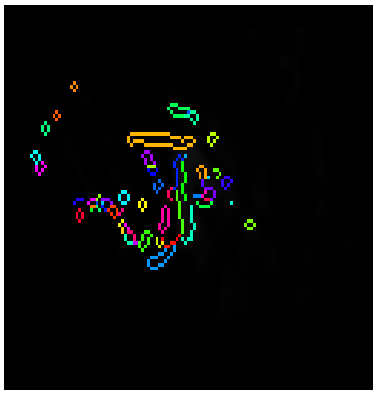
IM0270	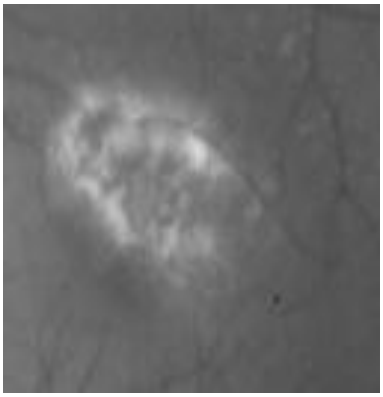	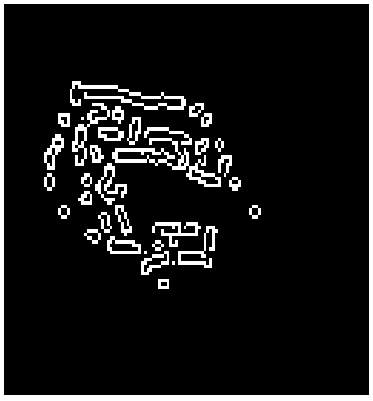	

IM0281	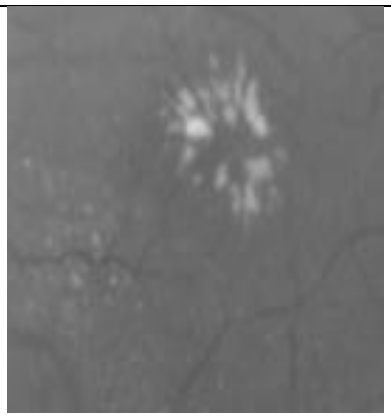	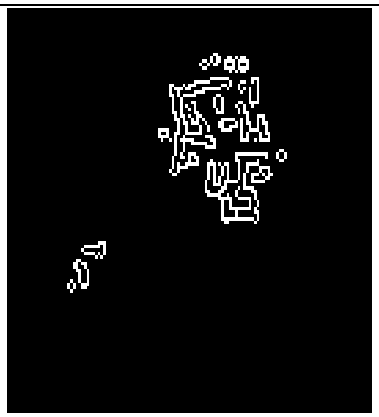	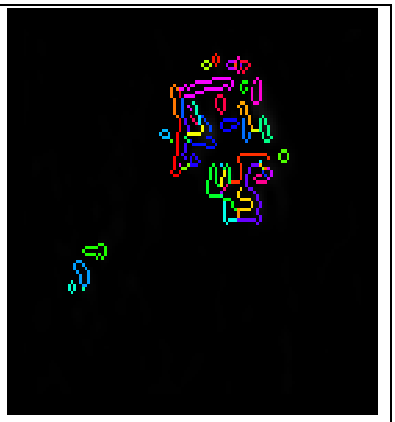
IM0382	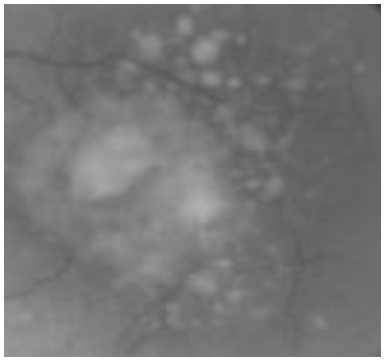		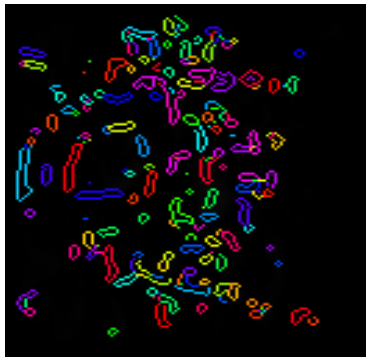
IM0401	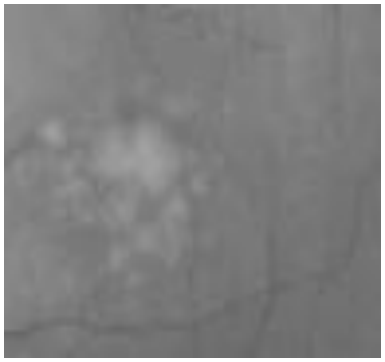	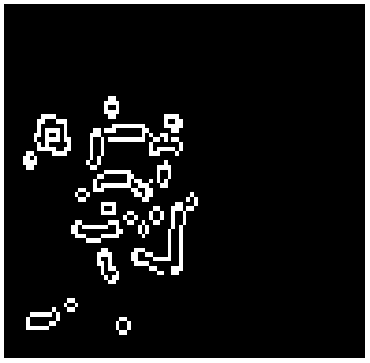	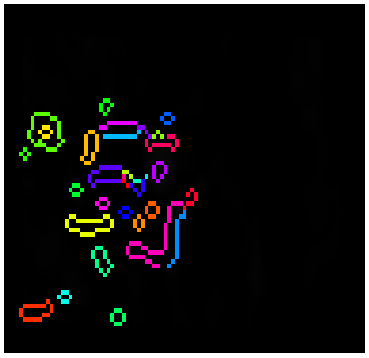
IM0402		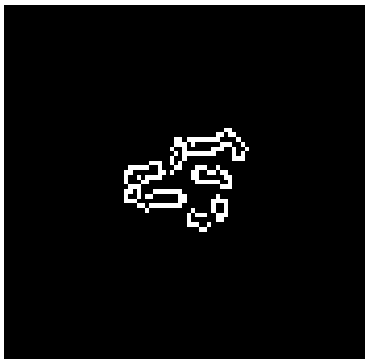	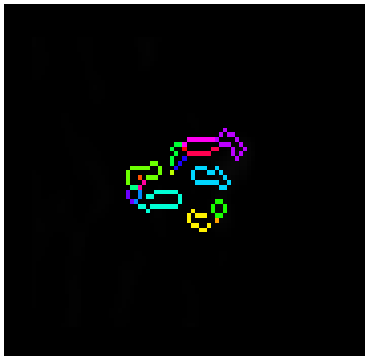

Figure 7.0: Results of detected boundary of drusen; column 1 showing list of images; column 2 showing text images; column 3 showing boundary of drusen; column 4 showing pseudo color indexed images

6.2.4 Grading of AMD

It categorizes drusen into small, intermediate and large on the basis of drusen size, area and number to find the stages of AMD for further diagnosis.

Table 6.2: Classification and Quantitative analysis of drusen to grade the severity of AMD for Method 2

	IMAGES	**Total no. Of drusen by the ground truth**	**Total drusen area in the ground truth (μm^2)**	**Size of drusen (μm)**	**Total no. Of drusen by the proposed method**	**Total drusen area by the proposed method μm^2**	**Size of drusen in μm**
SMALL	IM0013	4	74.584	45.508	4	74.854	45.508
	IM0015	15	95.266	39.627	13	91.985	32.471
	IM0039	9	77.542	23.521	8	76.447	36.777
	IM0159	2	$1.188X10^{10}$	18.785	2	$1.153X10^{10}$	18.785
	IM0219	3	$1.728X10^{10}$	63.923	3	$1.635X10^{10}$	62.500
	IM0220	2	20.982	29.094	2	18.231	29.004
	IM0239	3	40.689	27.225	3	39.936	27.176
	IM0244	6	37.967	18.937	6	33.329	16.668
	IM0262	13	$2.375X10^{10}$	52.829	12	$1.997X10^{10}$	51.064
	IM0401	16	$1.317X10^{10}$	48.752	14	$1.188X10^{10}$	48.418
	IM0402	5	$1.173X10^{10}$	25.975	5	$1.021X10^{10}$	25.135

	IMAGES	Total no. Of drusen by the ground truth	Total drusen area in the ground truth (μm^2)	Size of drusen (μm)	Total no. Of drusen by the proposed method	Total drusen area by the proposed method μm^2	Size of drusen in μm
INTERMEDIATE	IM0012	113	$1.498X10^{11}$	74.002	110	$1.363X10^{11}$	73.975
	IM0046	7	63.846	97.899	7	63.846	59.899
	IM0066	80	$2.209X10^{10}$	103.981	80	$2.208X10^{10}$	103.981
	IM0068	125	$1.689X10^{10}$	63.932	125	$1.653X10^{10}$	63.500
	IM0069	90	$1.189X10^{10}$	187.854	90	$1.176X10^{10}$	187.854
	IM0142	120	$4.638X10^{11}$	65.712	120	$4.333X10^{11}$	65.616
	IM0192	136	$2.603X10^{12}$	118.295	134	$2.471X10^{12}$	118.268
	IM0193	150	$3.081X10^{11}$	85.360	149	$2.908X10^{11}$	82.020
	IM0206	4	30.328	105.957	4	29.576	105.833
	IM0263	89	$1.759X10^{10}$	72.654	86	$1.508X10^{10}$	72.652
	IM0286	118	$2.598X10^{11}$	124.621	112	$2.095X10^{11}$	124.618
	IM0376	2	90.985	127.541	2	90.977	127.541
	IM0381	72	$2.896X10^{11}$	77.938	69	$2.229X10^{11}$	77.787

	IMAGES	Total no. Of drusen by the ground truth	Total drusen area in the ground truth (μm^2)	Size of drusen (μm)	Total no. Of drusen by the proposed method	Total drusen area by the proposed method μm^2	Size of drusen in μm
LARGE or SOFT DRUSEN	IM0062	10	$3.183X10^{11}$	265.237	10	$3.170X10^{11}$	265.125
	IM0063	76	$3.679X10^{10}$	248.521	62	$3.006X10^{10}$	248.708
	IM0097	110	$2.833X10^{11}$	166.278	95	$1.234X10^{11}$	162.687
	IM0098	139	$1.255X10^{11}$	151.002	130	$1.034X10^{11}$	149.812
	IM0143	27	$9.484X10^{10}$	336.125	27	$9.484X10^{10}$	336.020
	IM0147	33	$3.329X10^{11}$	183.613	33	$3.332X10^{11}$	183.521
	IM0148	41	$5.113X10^{11}$	82.366	41	$5.039X10^{11}$	82.285
	IM0149	43	$3.002X10^{11}$	412.97	43	$2.926X10^{11}$	412.75
	IM0229	29	$2.587X10^{10}$	262.157	27	$2.171X10^{10}$	261.937
	IM0250	104	$4.595X10^{10}$	595.062	100	$4.559X10^{10}$	595.047
	IM0259	16	46.578	137.95	16	46.563	134.90
	IM0265	43	$1.386X10^{10}$	176.24	40	$1.201X10^{10}$	174.625
	IM0266	101	$7.283X10^{10}$	559.68	96	$6.935X10^{10}$	538.27
	IM0267	117	$1.602X10^{11}$	679.252	112	$1.496X10^{10}$	669.395
	IM0269	49	56.749	135.925	49	54.980	134.143
	IM0270	10	$5.174X10^{10}$	152.231	10	$5.165X10^{10}$	152.135
	IM0271	26	$7.132X10^{10}$	119.565	26	$7.084X10^{10}$	119.327
	IM0281	31	$2.219X10^{10}$	569.013	31	$2.218X10^{10}$	560.916
	IM0288	40	$4.082X10^{11}$	146.522	36	$3.698X10^{11}$	143.366
	IM0332	85	$1.255X10^{12}$	503.995	70	$1.003X10^{12}$	498.766
	IM0338	221	$8.644X10^{11}$	138.929	119	$6.988X10^{11}$	136.906
	IM0382	82	$2.676X10^{11}$	445.22	82	$2.580X10^{11}$	444.50
	IM0383	116	$5.073X10^{11}$	139.236	114	$4.998X10^{11}$	137.583

6.2.5 Performance evaluation parameters

In order to establish the performance of the proposed method, statistical measures such as rate of true positive detection (sensitivity), rate of true negative detection (specificity), accuracy, MCC and PPV have been computed and validated by examining pixel-to-pixel comparison with ground truth. The summary of statistics ($mean \pm standard\ deviation$) of all 48 images is shown in the form of box plots. Fig. 7.1 summarizes the overall performance of the method 2 with standard databases. It depicts that the drusen detection method achieved sensitivity, specificity, accuracy, MCC and PPV as (89.81 ± 14.26) %, (97 ± 0.98)%, (96.17 ± 5.41)%, (95.94 ± 5.57)% and (96.4 ± 5.09)%respectively. Fig. 6.3 (b) shows that the sensitivity and specificity, accuracy, MCC and PPV of method 1 are (82 ± 16.52) %, (91.3 ± 1.13)%, (93.2 ± 2.42)%, (92.21 ± 7.2)% and (95 ± 6.31)% respectively. Fig. 7.1 (c) and (d) shows the comparison of performance parameter between method 2 and method 1 for STARE database. It illustrates that the performance parameters for method 2 are 88.95 %, 95.24%, 95.48%, 93.2% and 94.12% respectively and for method 1 it is 81.5% for sensitivity, 87.5% for specificity, 87.93% for accuracy, 83.76% for PPV and 83.71% for MCC respectively. Fig. 7.1 (e) and (f) shows the comparison of performance parameter between method 2 and method 1 for ARIA database. It illustrates that the performance parameters for method 2 are 83.5 %, 96.14%, 91%, 91.18% and 96.6% respectively and for method 1 it is 76% for sensitivity, 92.5% for specificity, 82.2% for accuracy, 85.67% for PPV and 83.1% for MCC respectively.

In the literature, only few methods [63] considered the speed (execution time) for the detection and quantification of drusen using fundus images. Bhuiyan et al. showed in their work, the execution time to process a single image is less than 0.5 second to quantify the drusen area [63].None of any other methods in the literature paid attention to the time complexity of the algorithm. The method 2 takes approximately 0.218 seconds to process a single image for the quantification and it may vary image to image depends on the size and color effects. In addition to that, the execution time (approximately) 0.0738 seconds for boundary detection, 0.251 seconds for edge tracking in 271 iterations, 0.385 seconds for edge linking of available pixels in 3246 iterations and 103.353 seconds

for total execution time of the method. Whereas, method 1 takes 175.093 seconds for total execution time and 0.048 seconds for edge detection and 0.042 seconds for area quantification only. There is a 70% (from 175.093 to 103.353) time complexity reduction from the method 1 to that of method 2. Also method 2 outperforms the other state of art method by achieving high values of accuracy for grading as compared to other methods. This improvement is especially in terms of PPV and MCC for drusen boundary detection which is supported by accurately detecting the candidate drusen boundary by suppressing the spurious regions, result in lower number of false positives. The method 2 has less false positive comparatively to other existing methods.

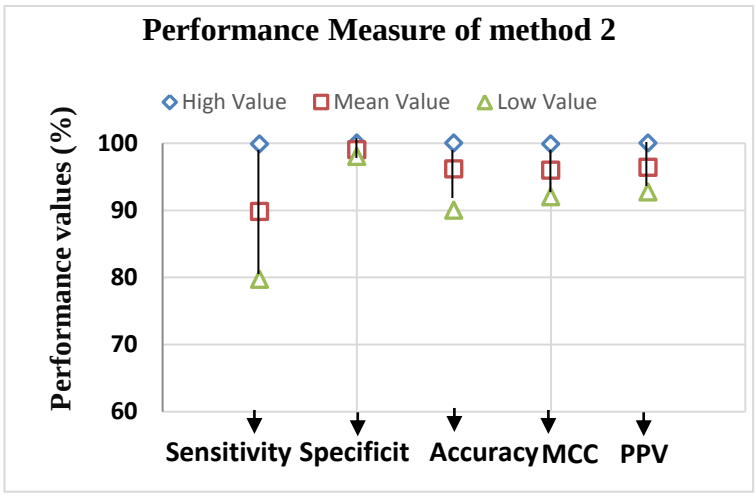

(a)

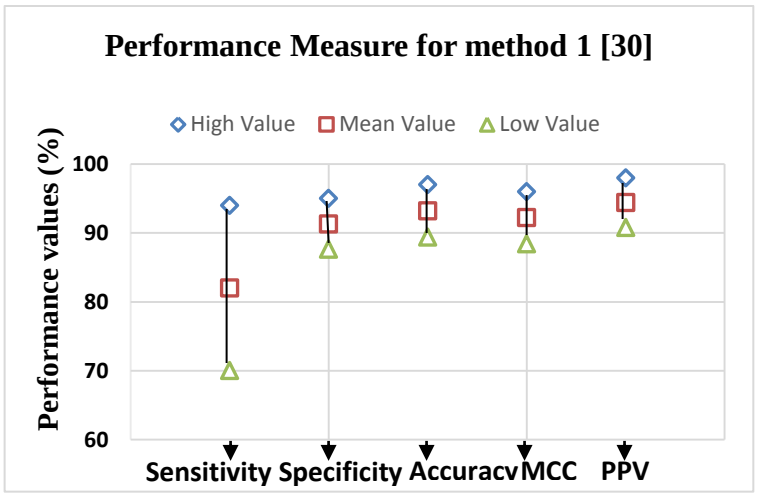

(b)

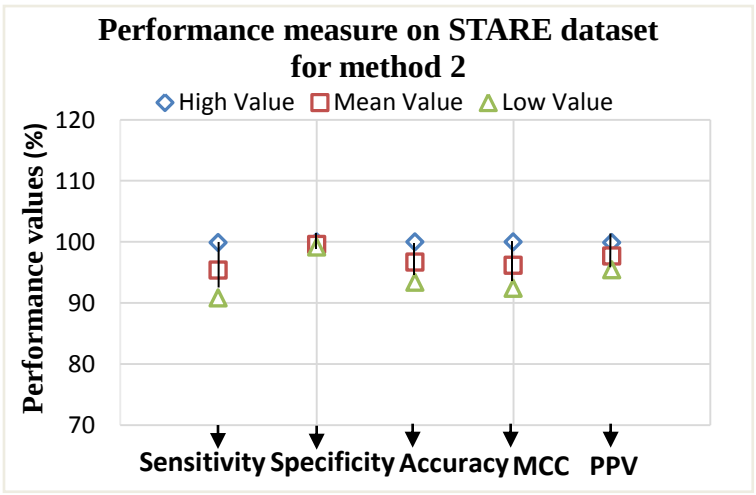

(c)

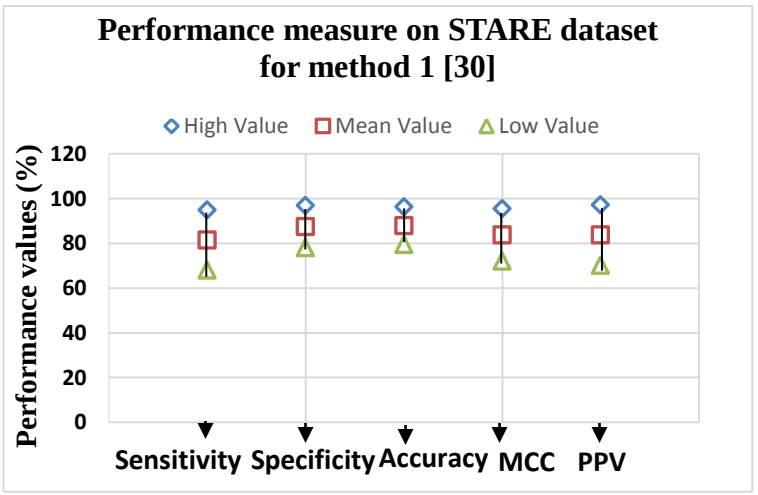

(d)

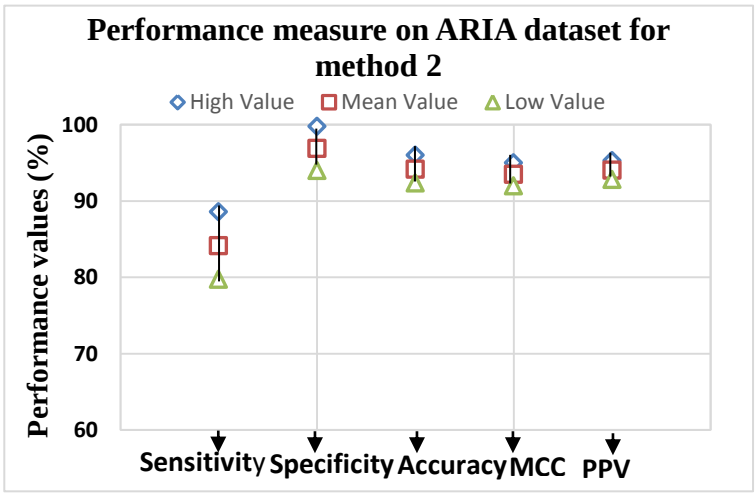

(e)

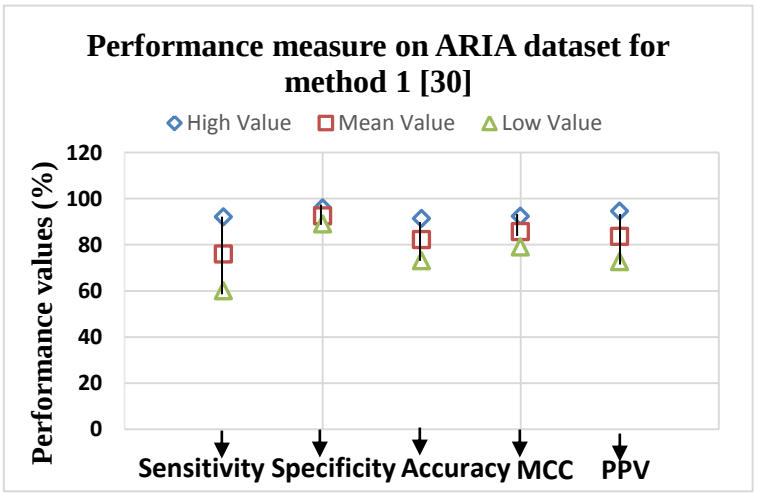

(f)

Figure 7.1: Box plot for performance measure of method 1 and 2

Chapter – 7

CONCLUSION AND FUTURE WORK

7.1 Conclusion

This thesis presented two methodologies for automatic detection and quantification of drusen deposits in retinal images using digital image processing techniques. The automation of such task allowed reproducible and accurate measurements to be made without user intervention. This will help in grading the severity of AMD to assess drusen progression. For ophthalmologists the existence of such tool will contribute to a better understanding of drusen progression and early assessment of drusen changes, since the quantitative analysis of drusen helped in assessing the stages of AMD by finding the size, number and area of drusen.

A literature review on automated drusen detection showed that most of the existing methods did not use quantitative analysis for grading the AMD severity, which is an important step to diagnose it. Therefore, the strategy in this work was to exploit other image processing techniques to solve this problem. There are two different types of methodologies which are employed to find the boundary of drusen and further help in grading the severity of AMD. These were divided into four steps: image pre-processing, drusen detection, drusen quantification and grading have been validated by comparing it with the ground truth.

In this work, an automated detection of drusen using publicly available retinal fundus images is proposed. In the first method, region and custom properties of image are analyzes by extracting the feature from the pixels of fundus images. This algorithm will help in computing the total area affected by drusen in pixels with its edge. Centre of mass (weighted centroid) with standard deviation is used to separate out different objects which help in calculating total number of drusen present in image. Use of the proposed detector may reduce false negatives and give reliable results in both area and number of drusen. In the second method, the proposed system presented a method for drusen boundary detection by suppressing the spurious region based on gradient and assembling

the edge pixels with same label to form a meaningful boundary and quantify it according to its size, area and number which will further helped in grading.

The performance, in terms of the execution time, was a concern for this thesis. The objective was to create algorithms that could be easily introduced in medical assisting tools, which optimizes performance of the algorithm.

To assess the accuracy of the methodologies in quantifying drusen, different types of parameters are used. From the statistical analysis of the agreement with the ground truth, it is concluded that the algorithm achieved sensitivity of 95.74%, specificity of 98.97%, accuracy of 97.76%, PPV of 97.18% and MCC of 98.65% with computation cost of 103. 353 seconds, can be compared with the published results and almost equal to the performance of human observers. The method has been evaluated and compared with the database images of STARE and ARIA on both the test and training images both containing 48 images.

From general and clinical analysis of this work, it can be said that the proposed methodology is able to detect and quantify drusen which further help in grading the severity of AMD using an automated procedure.

7.2 Future Aspects

- This methodology can be applied on SD-OCT images in future.
- Size of distinguishable and indistinguishable drusen can be evaluated.

REFERENCES

[1] World Health Organization. "Global Initiative for the Elimination of Avoidable Blindness: action plan 2006-2011." (2007).

[2] De Jong, Paulus TVM. "Age-related macular degeneration." *New England Journal of Medicine* 355.14 (2006): 1474-1485.

[3] World Health Organization. Fact Sheet No. 144. *Blindness and Visual Disability*. Part III of VII: Other Leading Causes Worldwide. Available at URL: (worldwide.www.who.int/inf-fs/en/fact144html). Accessed 4 july 2013.

[4] Arakawa, Satoshi, et al. "Genome-wide association study identifies two susceptibility loci for exudative age-related macular degeneration in the Japanese population." *Nature genetics* 43.10 (2011): 1001-1004.

[5] Wang, Jie Jin, et al. "Ten-year incidence and progression of age-related maculopathy: the Blue Mountains Eye Study." *Ophthalmology* 114.1 (2007): 92-98.

[6] Rajan, S. Irudaya, P. Sankara Sarma, and U. S. Mishra. "Demography of Indian aging, 2001-2051." *Journal of aging & social policy* 15.2-3 (2003): 11-30.

[7] Wong, Tien Y., Gerald Liew, and Paul Mitchell. "Clinical update: new treatments for age-related macular degeneration." *The Lancet* 370.9583 (2007): 204-206.

[8] Wong, Tien Y., and Sophie L. Rogers. "Statins and age-related macular degeneration: time for a randomized controlled trial?." *American journal of ophthalmology* 144.1 (2007): 117-119.

[9] Wade, Nicholas J. Image, eye, and retina (invited review). *Journal of the Optical Society of America. A, Optics, image science, and vision 24*, 5 (2007), 1229–1249.

[10] Abramoff, Michael D., Mona K. Garvin, and Milan Sonka. "Retinal imaging and image analysis." Biomedical Engineering, IEEE Reviews in 3 (2010): 169-208.

[11] Abràmoff, Michael D., et al. "Automated early detection of diabetic retinopathy." *Ophthalmology* 117.6 (2010): 1147-1154.

[12] Cassin, B., and S. A. B. Solomon. "Dictionary of Eye Terminology. 1990."*Triad, Gainesville (FL)*.

[13] Von Helmholtz, Hermann Ludwig Ferdinand. *The Description of an ophthalmoscope*. Cleveland Press, 1916.

[14] Saine, P. J. "Fundus photography: What is a fundus camera." *Ophthalmic Photographers' Society.(Cited in section 2.1. 2.)* (2006).

[15] Walsh, A. C., et al. "Detection of fundus abnormalities using 3d-oct versus mydriatic color fundus imaging." *Investigative Ophthalmology & Visual Science*51.13 (2010): 3863-3863.

[16] Chang, A. A., et al. "Indocyanine green localisation in surgically excised choroidal neovascular membrane in age related macular degeneration." *British journal of ophthalmology* 88.2 (2004): 307-309.

[17] Schmitz-Valckenberg, Steffen, et al. "Fundus autofluorescence imaging: review and perspectives." *Retina* 28.3 (2008): 385-409.

[18] Davis, Bert, et al. "Identification of spectral phenotypes in age-related macular degeneration patients." *Biomedical Optics (BiOS) 2007*. International Society for Optics and Photonics, 2007.

[19] Klein, Ronald, et al. "The Wisconsin age-related maculopathy grading system."*Ophthalmology* 98.7 (1991): 1128-1134.

[20] Bird, A. C., et al. "An international classification and grading system for age-related maculopathy and age-related macular degeneration." *Survey of ophthalmology* 39.5 (1995): 367-374.

[21] Choroidal Neovascularization Prevention Trial Research Group. "Laser treatment in eyes with large drusen: short-term effects seen in a pilot randomized clinical trial." *Ophthalmology* 105.1 (1998): 11-23.

[22] Age-Related Eye Disease Study Research Group. "A randomized, placebo-controlled, clinical trial of high-dose supplementation with vitamins C and E, beta carotene, and zinc for age-related macular degeneration and vision loss: AREDS report no. 8." *Archives of ophthalmology* 119.10 (2001): 1417.

[23] Seddon, J. M., et al. "Twin study of macular degeneration: Methodology and application to genetic epidemiologic studies." *INVESTIGATIVE OPHTHALMOLOGY & VISUAL SCIENCE*. Vol. 38. No. 4. 227 EAST WASHINGTON SQ, PHILADELPHIA, PA 19106: LIPPINCOTT-RAVEN PUBL, 1997.

[24] Seddon, Johanna M., et al. "A genomewide scan for age-related macular degeneration provides evidence for linkage to several chromosomal regions."*The American Journal of Human Genetics* 73.4 (2003): 780-790.

[25] Wang, Jie Jin, Paul Mitchell, and Ronald Klein. "Epidemiology of Age-Related Macular Degeneration Early in the 21st Century." *Retinal Degenerations*. Humana Press, 2007. 23-59.

[26] Schachat, Andrew P., et al. "Features of age-related macular degeneration in a black population." *Archives of ophthalmology* 113.6 (1995): 728-735.

[27] Frank, Robert N., et al. "Race, iris color, and age-related macular degeneration." *Transactions of the American Ophthalmological Society* 98 (2000): 109.

[28] Sandberg, Michael A., et al. "High-risk characteristics of fellow eyes of patients with unilateral neovascular age-related macular degeneration." *Ophthalmology*105.3 (1998): 441-447.

[29] Cukras, Catherine, and Fredrick Ferris. "Cardiovascular Risk Factors And Age-Related Macular Degeneration: The Los Angeles Latino Eye Study." *Evidence-Based Ophthalmology* 9.3 (2008): 193-194.

[30] Seddon, Johanna M., Sarah George, and Bernard Rosner. "Cigarette smoking, fish consumption, omega-3 fatty acid intake, and associations with age-related macular degeneration: the US Twin Study of Age-Related Macular Degeneration." *Archives of Ophthalmology* 124.7 (2006): 995-1001.

[31] Fletcher, Astrid E., et al. "Sunlight exposure, antioxidants, and age-related macular degeneration." *Archives of ophthalmology* 126.10 (2008): 1396-1403.

[32] Vingerling, Johannes R., et al. "Age-related macular degeneration and smoking: the Rotterdam Study." *Archives of ophthalmology* 114.10 (1996): 1193-1196.

[33] Pauleikhoff, D., et al. "Drusen as risk factors in age-related macular disease."*American journal of ophthalmology* 109.1 (1990): 38-43.

[34] Johnson, Patrick T., et al. "Drusen-associated degeneration in the retina."*Investigative ophthalmology & visual science* 44.10 (2003): 4481-4488.

[35] Brandon, Lee, and Adam Hoover. "Drusen detection in a retinal image using multi-level analysis." *Medical Image Computing and Computer-Assisted Intervention-MICCAI 2003*. Springer Berlin Heidelberg, 2003. 618-625.

[36] Parvathi, S. Swarna, and N. Devi. "Automatic drusen detection from colour retinal images." *Conference on Computational Intelligence and Multimedia Applications, 2007. International Conference on*. Vol. 2. IEEE, 2007.

[37] Lee, Noah, Andrew F. Laine, and Theodore R. Smith. "Learning non-homogenous textures and the unlearning problem with application to drusen detection in retinal images." *Biomedical Imaging: From Nano to Macro, 2008. ISBI 2008. 5th IEEE International Symposium on*. IEEE, 2008.

[38] Barriga, Eduardo S., et al. "Multi-scale AM-FM for lesion phenotyping on age-related macular degeneration." *Computer-Based Medical Systems, 2009. CBMS 2009. 22nd IEEE International Symposium on*. IEEE, 2009.

[39] Freund, David E., Neil Bressler, and Philippe Burlina. "Automated detection of drusen in the macula." *Biomedical Imaging: From Nano to Macro, 2009. ISBI'09. IEEE International Symposium on*. IEEE, 2009.

[40] Köse, Cemal, et al. "A statistical segmentation method for measuring age-related macular degeneration in retinal fundus images." *Journal of Medical Systems* 34.1 (2010): 1-13.

[41] Agurto, Carla, et al. "Automatic detection of diabetic retinopathy and age-related macular degeneration in digital fundus images." *Investigative ophthalmology & visual science* 52.8 (2011): 5862.

[42] Priya, R., and P. Aruna. "Automated diagnosis of Age-related macular degeneration from color retinal fundus images." *Electronics Computer Technology (ICECT), 2011 3rd International Conference on*. Vol. 2. IEEE, 2011.

[43] Prasath, A. Rama, and N. L. M. Ramya. "Detection of Macular Drusen Based On Texture Descriptors." *Research Journal of Information Technology* 7.1 (2015): 70-79.

[44] Mookiah, Muthu Rama Krishnan, et al. "Automated diagnosis of Age-related Macular Degeneration using greyscale features from digital fundus images."*Computers in biology and medicine* 53 (2014): 55-64.

[45] Morgan, William H., et al. "Automated extraction and quantification of macular drusen from fundal photographs." *Australian and New Zealand Journal of Ophthalmology* 22.1 (1994): 7-12.

[46] Rapantzikos, Konstantinos, and Michalis Zervakis. "Nonlinear enhancement and segmentation algorithm for the detection of age-related macular

degeneration (AMD) in human eye's retina." *Image Processing, 2001. Proceedings. 2001 International Conference on*. Vol. 3. IEEE, 2001.

[47] Soliz, Peter, et al. "Computer-aided methods for quantitative assessment of longitudinal changes in retinal images presenting with maculopathy." *Medical Imaging 2002*. International Society for Optics and Photonics, 2002.

[48] Smith, R. Theodore, et al. "A method of drusen measurement based on the geometry of fundus reflectance." *Biomedical engineering online* 2.1 (2003): 10.

[49] Barakat, M. R., and B. Madjarov. "Automated drusen quantitaion for clinical trials." *Investigative Ophthalmology & Visual Science*. Vol. 45. 12300 Twinbrook Parkway, Rockville, Md 20852-1606 Usa: Assoc Research Vision Ophthalmology Inc, 2004.

[50] Smith, R. Theodore, et al. "Automated detection of macular drusen using geometric background leveling and threshold selection." *Archives of ophthalmology* 123.2 (2005): 200-206.

[51] Liang, Ziyang, et al. "Towards automatic detection of age-related macular degeneration in retinal fundus images." *Engineering in Medicine and Biology Society (EMBC), 2010 Annual International Conference of the IEEE*. IEEE, 2010.

[52] O. Sheeba and Vinayan Nikki. Image segmentation and analysis in the case study of macular degeneration using Labview. *Intern J of Engg and Adv Techn*. 2013; 3: 14-17.

[53] Ramya, M. M. "Automatic detection and elimination of an optic disc for improving drusen detection accuracy." *Signal and Image Processing (ICSIP), 2014 Fifth International Conference on*. IEEE, 2014.

[54] Kumari, Kajal, and Deepti Mittal. "Automated Drusen Detection Technique for Age-Related Macular Degeneration." *Journal of Biomedical Engineering and Medical Imaging* 2.1 (2015): 18.

[55] Hijazi, Mohd Hanafi Ahmad, Frans Coenen, and Yalin Zheng. "Retinal image classification for the screening of age-related macular degeneration." *Research and Development in Intelligent Systems XXVII*. Springer London, 2011. 325-338.

[56] Quellec, Gwenole, Stephen R. Russell, and Michael D. Abràmoff. "Optimal filter framework for automated, instantaneous detection of lesions in retinal images."*Medical Imaging, IEEE Transactions on* 30.2 (2011): 523-533.

[57] Raza, Ghazanfar, et al. "Hybrid classifier based drusen detection in colored fundus images." *Applied Electrical Engineering and Computing Technologies (AEECT), 2013 IEEE Jordan Conference on*. IEEE, 2013.

[58] Zhang, Li, et al. "Automated segmentation of the choroid from clinical SD-OCT." *Invest Ophthalmol Vis Sci* 53.12 (2012): 7510-7519.

[59] Hijazi, Mohd Hanafi Ahmad, Frans Coenen, and Yalin Zheng. "Age-Related Macular Degeneration Screening Using Data Mining Approaches." *Artificial Intelligence, Modelling and Simulation (AIMS), 2013 1st International Conference on*. IEEE, 2013.

[60] Mookiah, Muthu Rama Krishnan, et al. "Decision support system for age-related macular degeneration using discrete wavelet transform." *Medical & biological engineering & computing* 52.9 (2014): 781-796.

[61] Remeseiro, Beatriz, et al. "Automatic drusen detection from digital retinal images: Amd prevention." *Computer Aided Systems Theory-EUROCAST 2009*. Springer Berlin Heidelberg, 2009. 187-194.

[62] Mora, André D., et al. "Automated drusen detection in retinal images using analytical modelling algorithms." *Biomedical engineering online* 10.1 (2011): 59.

[63] Bhuiyan, Alauddin, et al. "Drusen detection and quantification for early identification of age related macular degeneration using color fundus imaging."*J. Clin. Exp. Ophthalmol* 4.305 (2013): 2.

[64] Gonzalez, Rafael C., and Richard E. Woods. "Digital image processing 3rd edition." (2007).

[65] Fan, Chun-Nian, and Fu-Yan Zhang. "Homomorphic filtering based illumination normalization method for face recognition." *Pattern Recognition Letters* 32.10 (2011): 1468-1479.

[66] Adelmann, Holger G. "Butterworth equations for homomorphic filtering of images." *Computers in Biology and Medicine* 28.2 (1998): 169-181.

[67] Canny, John. "A computational approach to edge detection." *Pattern Analysis and Machine Intelligence, IEEE Transactions on* 6 (1986): 679-698.

[68] Ghita, Ovidiu, and Paul F. Whelan. "Computational approach for edge linking."*Journal of Electronic Imaging* 11.4 (2002): 479-485.

[69] STARE database. Available at http://www.ces.clemson.edu/~ahoover/stare.

[70] ARIA database. Available athttp://www.eyecharity.com/aria_online.

[71] Kumari, Kajal, and Deepti Mittal. "Drusen Quantification for Early Identification of Age Related Macular Degeneration." *Advances in Image and Video Processing"* 3.3 (2015): 28-40.